HHS Public Access

Author manuscript

Brain Behav Immun. Author manuscript; available in PMC 2018 March 01.

Published in final edited form as:

Brain Behav Immun. 2017 March ; 61: 80–95. doi:10.1016/j.bbi.2016.12.016.

Prenatal alcohol exposure potentiates chronic neuropathic pain, spinal glial and immune cell activation and alters sciatic nerve and DRG cytokine levels

Shahani Noor[1], **Joshua J. Sanchez**[1,**], **Arden G. Vanderwall**[1,2,**], **Melody S. Sun**[1], **Jessie R. Maxwell**[3], **Suzy Davies**[1], **Lauren L. Jantzie**[1,3], **Timothy R. Petersen**[2], **Daniel D. Savage**[1,3], and **Erin D. Milligan**[1]

[1]Department of Neurosciences, School of Medicine, University of New Mexico Health Sciences Center, Albuquerque, NM, 87131-0001, USA

[2]Department of Anesthesiology and Critical Care Medicine, University of New Mexico Health Sciences Center, Albuquerque, NM, 87131-0001, USA

[3]Department of Pediatrics, University of New Mexico Health Sciences Center, Albuquerque, NM, 87131-0001, USA

Abstract

A growing body of evidence indicates that prenatal alcohol exposure (PAE) may predispose individuals to secondary medical disabilities later in life. Animal models of PAE reveal neuroimmune sequelae such as elevated brain astrocyte and microglial activation with corresponding region-specific changes in immune signaling molecules such as cytokines and chemokines. The aim of this study was to evaluate the effects of moderate PAE on the development and maintenance of allodynia induced by chronic constriction injury (CCI) of the sciatic nerve in adult male rat offspring. Because CCI allodynia requires the actions of glial cytokines, we analyzed lumbar spinal cord glial and immune cell surface markers indicative of their activated levels, as well as sciatic nerve and dorsal root ganglia (DRG) cytokines in PAE offspring in adulthood. While PAE did not alter basal sensory thresholds before or after sham manipulations, PAE significantly potentiated adult onset and maintenance of allodynia. Microscopic analysis revealed exaggerated astrocyte and microglial activation, while flow cytometry data demonstrated increased proportions of immune cells with cell surface major histocompatibility complex II (MHCII) and β-integrin adhesion molecules, which are indicative of PAE-induced immune cell activation. Sciatic nerves from CCI rats revealed that PAE potentiated the proinflammatory cytokines interleukin (IL)-1β, IL-6 and tumor necrosis factor-alpha (TNFα) protein levels with a simultaneous robust suppression of the anti-inflammatory cytokine, IL-10. A

*Corresponding author: EMilligan@salud.unm.edu. Mailing address: MSC08 4740, 1 University of New Mexico, Albuquerque, NM 87131-0001, Office Tel: +1 (505) 272-8103, Lab Tel: +1 (505) 272-4441, Fax: +1 (505) 272-8082.

**These authors contributed equally to this work.

Conflict of Interest statement

The authors declare no conflict of interest.

profound reduction in IL-10 expression in the DRG of PAE neuropathic rats was also observed. Taken together, our results provide novel insights into the vulnerability that PAE produces for adult-onset central nervous system (CNS) pathological conditions from peripheral nerve injury.

Keywords

neuropathic pain; chronic constriction injury; β-integrin adhesion molecules; prenatal alcohol exposure; Fetal Alcohol Spectrum Disorder; inflammatory cytokines; spinal glia; astrocytes; microglia; sciatic nerve; neuroimmune interactions

1. Introduction

Fetal alcohol spectrum disorder (FASD) encompasses a continuum of disabilities that includes a range of cognitive and behavioral deficits [53]. Impairments in neurogenesis, motor and memory performance and neurotransmitter activity in various brain regions are consistently observed in studies using animal models of moderate PAE where peak maternal serum alcohol concentrations in the range of ≤0.02 – 0.17 g/dl are achieved. Despite the US legal intoxication limit while operating vehicles is 0.08g/dl blood alcohol concentration (for review, [104]), lower blood alcohol concentration levels may still impair cognitive and behavioral performance in adults [13,35,36,84]. In rat and rhesus monkey, moderate PAE models that utilize a voluntary drinking paradigm impair performance on hippocampal-, cerebellar-, and cortical-dependent behavioral tasks [2,5,15,20,43,83,86]. Curiously, PAE in rhesus monkeys reveal significant hypersensitivity to light touch [85,87], suggesting impairment of sensory relays in the spinal cord from incoming peripheral nerve fibers.

Evidence is accumulating that PAE significantly impacts CNS immune function. Several studies demonstrate PAE primes glial cell reactivity in the brain. Elevated proinflammatory chemokine and cytokine levels in PAE rats are observed in different brain regions for weeks to several months after birth [3,12,27,100,102,103]. Recent studies indicate that PAE may alter the immune response to subsequent brain injury in adulthood. For example, following a brain stab wound, macrophages, microvascular endothelial cells and microglia are markedly activated in PAE rats [27]. Clinically, less is known about the impact of PAE on adult CNS immune function. However, one study reported elevated circulating proinflammatory cytokines in PAE neonates [1] and clinicians have long observed that children with developmental disabilities display tactile hypersensitivity [9,34]. While speculative, tactile hypersensitivity may extend to individuals with FASD.

In animal models of peripheral neuropathy, such as unilateral chronic constriction injury (CCI) of the rodent sciatic nerve [11], low threshold tactile hypersensitivity, also called allodynia (for review see [42,65,88]), is reliably observed [11,21,49]. In the CCI model, spinal astrocyte- and microglial-derived IL-1β and TNFα are well-characterized to excite nearby pain projection neurons [65]. In addition, the central projections of damaged sciatic nerves release CCL2 (C-C motif chemokine ligand 2 or macrophage chemotactic protein -1; MCP-1) [38], which further excites spinal glia and pain projection neurons. Evidence also supports the contribution of infiltrating leukocytes (i.e. monocytes/macrophages and $CD4^+$ T cells) to allodynia in response to spinal CCL2-CCR2 signaling [17,22,97]. The adhesion

molecules, lymphocyte function-associated antigen 1 (LFA-1), macrophage-1 antigen (Mac-1) and very late antigen-4/VLa4) [29,75], as well as MHCII facilitate immune cell trafficking, proliferation and differentiation (for review [112]). Damaged sciatic nerve axons from CCI induce peri-sciatic expression of IL-1β, IL-6 and TNFα and chemokines from accumulating immune cells [71,72,78,79,88,99], which can generate compensatory anti-inflammatory interleukin-10 (IL-10) [54,88] cytokine increases.

Given the existing evidence supporting the negative impact of immune-mediated conditions underlying peripheral nervous system (PNS) and/or CNS pathology observed from both PAE [53] and from chronic peripheral neuropathic pain [65], we examined whether moderate PAE potentiated allodynia and corresponding spinal glial and immune cell β-integrin and MHCII expression following peripheral nerve CCI in a rat model. Further, the corresponding sciatic nerve and DRG, anatomically-relevant nociceptive regions, were examined for pro- and anti-inflammatory cytokines levels.

2. Materials and Methods

All procedures involving the use of live animals were approved by the University of New Mexico Health Sciences Center Institutional Animal Care and Use Committee and closely adhered to the guidelines from the International Association for the Study of Pain.

2.1. Study Group Strategy

Three independent experiments were conducted for behavioral assessment of hindpaw sensitivity followed by tissue collection as detailed here. Squad 1 was behaviorally assessed followed by experimental termination at Day 10 (N=6 rats/group) after surgical manipulation. The spinal cord enclosed within the vertebral column was collected from each rat for subsequent immunohistochemical (IHC) processing using decalcification and paraffin-embedding procedures as detailed below (2.4 Tissue preparation and immunohistochemistry). Due to prolonged decalcification processing, compromised tissue integrity occurred in some spinal cords resulting in reduced spinal cord samples per experimental condition (see Results, section 3.3). Prior work examining immunoreactive markers for spinal cord astrocytes and microglia following decalcification and paraffin-embedding procedures demonstrated N=3 spinal cords per experimental condition was sufficient to yield reliable group differences [110,111] and power analysis of the data obtained in this study confirmed that similar future studies would carry approximately 85.4% power. Squad 2 was conducted to (a) replicate behavioral hindpaw responses observed in the initial study described above, and (b) determine whether non-decalcified and non-paraffin-embedded tissue processing methods (detailed in 2.4 Tissue preparation and immunohistochemistry) yielded similar microglial and astrocyte immunoreactivity as observed in squad 1. For squad 2, N=4 rats were used in each experimental condition with hind paw behavioral assessment occurring until Day 10 followed by spinal cord dissection and cryosectioning. The data from behavioral hindpaw responses from squads 1 and 2 were combined resulting in N=10 rats per experimental condition. A third group (squad 3) examined hindpaw response thresholds that extended beyond Day 10 post-surgery to determine whether potentiated allodynia persisted. On Day 28 after sham or CCI surgery and

following behavioral assessment, peripheral tissues and spinal cords were examined to characterize immune related cell surface markers and cytokine expression profiles. While squad 3 initially consisted of N=6 rats per experimental condition for a total of 24 animals, attrition (N=3 total) occurred reducing the number of animals in some experimental groups (see Results, section 3.4). Upon observing autotomy (self-mutilation of the ipsilateral hindpaw toes), rats are immediately withdrawn from the study and euthanized (N=3 total observed in squad 3). Thus, the representative rat numbers for squad 3 were saccharin sham N=5, saccharin CCI N=5, PAE sham N=6, and PAE CCI N=4. Tissues from all rats from squad 3, were used for flow cytometric analysis of discrete immune markers, which in some cases were limited by their availability for rat-specific antibodies conjugated to appropriate fluorophores for flow cytometric detection.

2.2. Prenatal Alcohol Exposure Paradigm

Long-Evans rats (Harlan Industries, Indianapolis, IN, USA) housed at 22 °C on a reverse 12-hour dark/12-hour light schedule (lights on from 2100 to 0900 hours) and provided Harlan Tekland rodent chow and tap water *ad libitum*. After one-week of acclimation to the animal facility, three- to four-month old rat Harlan breeders were exposed to a voluntary drinking paradigm as detailed previously by Savage et al. [83]. Briefly, all female breeders were single-housed and provided 0.066% (w/v) saccharin (Sac) in tap water for 4 hours each day from 1000 to 1400 hours. On Days 1–2, the Sac water contained 0% ethanol, and on Days 3–4, 2.5% (v/v) ethanol. On Day 5 and thereafter, Sac water contained 5% ethanol (v/v), and daily 4 hr consumption was determined for approximately 2 weeks for each female breeder. Females whose mean daily ethanol consumption was greater than one standard deviation above or below the group mean (~12–15% of the entire group) were removed from the study. The remaining females were then assigned to either a Sac control (0% ethanol) or 5% ethanol (v/v) drinking group such that the mean ethanol consumption prior to pregnancy was similar between the two groups. Females were then placed with male breeders until pregnant, as indicated by the presence of a vaginal plug. The average days females became pregnant was 2.3 days.

Beginning on Gestational Day 1, rat dams were provided Sac water containing either 0% or 5% ethanol for four hours each day from 1000 to 1400 hours, with rodent chow and tap water provided at all times. The volume of Sac water provided to the control group was matched to the mean volume of Sac water consumed by the ethanol group. Daily four-hour ethanol consumption was recorded for each dam. At birth, litters were culled to ten pups each. Offspring were weaned at 24 days of age. Male offspring (2 taken from each litter producing 4–5 males/litter) from each prenatal treatment group were housed two per cage and transferred to the Milligan laboratory where they were maintained on a standard light-dark schedule and allowed to acclimate for at least three to four months prior to experimental procedures. Dams were allowed to become pregnant only once. To avoid a “litter effect”, offspring within a litter were assigned different experimental conditions, with no two rats from the same litter occurring within the same experimental condition.

2.3. Chronic constriction injury (CCI)

Four- to five-month-old adult male rat offspring from both the Sac control and PAE treatment groups were subjected to either sham or CCI aseptic surgical procedures as previously described [11] with minor modifications, as detailed elsewhere [111]. Briefly, under isoflurane anesthesia (induction 5% vol. followed by 3.5% in oxygen), the sciatic nerve was carefully isolated and ligated with 4 segments of 4-0 chromic gut sutures (Ethicon, Somerville, NJ) without pinching into the nerve. Sham surgery involved isolation of the sciatic nerve identical to CCI surgery but without nerve ligation. The overlying muscle was sutured closed with two 3–0 sterile silk sutures (Ethicon, Somerville, NJ), and rats fully recovered from anesthesia within approximately 5 min. Animals were monitored daily after surgery to ensure no complications from surgery occurred.

2.4. Behavioral Assessment of Allodynia

Three separate squads were assessed for allodynia using the von Frey fiber test. After rats were habituated to the testing environment, baseline (BL) responses were assessed as previously described [92]. Briefly, all rats were first habituated to the testing environment by placing rats atop 2-mm thick parallel bars spaced 8-mm apart allowing full access to the plantar hindpaw. Habituation occurred for approximately 45 min/day for 5 sequential days. All behavioral testing was performed during the first three hours of the light cycle in a sound-, light-, and temperature-controlled room. The von Frey behavioral test utilizes a series of calibrated monofilaments (2.44–5.18 log stimulus intensity) applied randomly to the left and right plantar surface of the hindpaw for a maximum of 8 seconds per application. Lifting, licking, or shaking of the paw was considered a response. In a similar manner to BL evaluation, animals in squads 1 and 2 were reassessed following CCI or sham surgery on Days 3 and 10 prior to tissue collection for procedures related to spinal IHC. Squad 3 rats were identically assessed for hindpaw threshold responses prior to and after CCI or sham surgery, on Days 3, 10, 15, 18, 23, and 28. The experimental tester was blind to the treatment groups.

2.5. Tissue preparation and Immunohistochemistry

Immediately after behavioral assessment on Day 10 post-surgery (Group 1 and 2), lumbar (L) 4–6 spinal cord segments were collected from both behaviorally-verified (hindpaw response thresholds) sham or CCI-treated rats and the tissues processed as described previously [27]. Briefly, rats were administered a lethal dose of sodium phenobarbital (Sleepaway, Fort Dodge Animal Health, Fort Dodge, IA) and underwent transcardial perfusion with 0.1M phosphate buffered saline (PBS; pH = 7.4) initially at 20 ml/min and completed at 24–28 ml/min (~10 min), followed by 4% paraformaldehyde (PFA; pH = 7.4; 28 ml/min, 8 min). Following transcardial perfusion, intact spinal vertebrae from C2-L6 were collected. The intact spinal vertebral column was hemisected at T7 generating a rostral and caudal half of the spinal vertebral column. All specimens underwent 24–48 hr post-fixation in 4% PFA. The next day, spinal cords from Squad 1 underwent decalcification of T7-L6 spinal vertebral column, with segments placed in 3 liters water containing 10% ethylenediaminetetraacetic acid (EDTA) (Sigma-Aldrich, St. Louis, MO) with 0.01% sodium azide and 0.5% paraformaldehyde with gentle consistent stirring atop a stir plate.

C2-T6 spinal segment were saved for future evaluation. The solution containing T7-L6 spinal vertebral column segments was exchanged every 5 days, with vertebral decalcification complete by 30 six months. The decalcified L4-L5 spinal cords were segmented and subsequently paraffin processed. L4-L5 paraffin-embedded blocks were then sliced on a microtome with 7μm tissue sections mounted onto vectabond-treated slides [107,111]. Given paraffin-processed spinal tissues had undergone decalcification for an extended period, we replicated the experimental conditions in Squad 1 but processed spinal tissues using non-decalcification methods. Thus, for comparison following perfusion as detailed above, lumbar spinal cords from a separate squad of rats (squad 2) representing each of the four identical experimental conditions (either sac or PAE with either sham or CCI; N=4/gp) were dissected from the vertebral column (L4-L6) and placed in standard Tissue-Tek cryomold containing Optimal Cutting Temperature (OCT) solution (Tissue-Tek, Torrance, CA, USA), flash frozen on dry ice and subsequently stored at −80°C until further processing. Sixteen μm-thick cryosections were mounted on Fisherbrand™ SuperFrost™ Plus slides. These tissues were stained using the identical glial activation markers (see below) to compare immunoreactivity between extended decalcification procedures and non-decalcified freshly dissected spinal cords.

To investigate spinal augmented glial activation, we analyzed the expression of the astrocyte marker, glial fibrillary acidic protein (GFAP) and the microglial activation marker Iba-1 (ionized calcium-binding adapter molecule) in L4-5 spinal segments as described in Wilkerson et al. [111] with the following brief modification. Randomly selected paraffin-processed L4-L5 mounted spinal cord tissue sections underwent deparaffinization followed by rehydration and microwave antigen retrieval procedures [111]. For antigen retrieval, Tris-based buffers, pH 9.5 (BioCare Medical, Concord, CA) was used for GFAP and pH 9 (Vector Laboratories, Burlingame, CA) was used for Iba-1 immunostaining.

For cryosectioned tissues from squad 2, randomly selected mounted spinal cord tissues were removed from −80 °C freezer and were allowed to warm up to room temperature for 30 minutes. Tissues were then post-fixed in 2% paraformaldehyde for 1 hour at room temperature. Tissue sections were then washed three times in 0.1M PBS (pH 7.4). Tissue sections were then was then incubated in 0.5% TritonX-100 in 0.1M PBS for 30 min with gentle rotation..

All tissue sections were incubated with 5% normal donkey serum (NDS), in PBS (pH 7.4) for 2h, followed by overnight primary antibody incubation (rabbit anti-rat GFAP, Millipore, 1:1000 dilution or rabbit anti-rat Iba-1, Wako, 1:300 dilution) in a humidity chamber at 4 °C. Tissues were washed three times with 0.1M PBS followed by donkey-anti rabbit TRITC (tetramethylrhodamine)-conjugated secondary antibody incubation for 2h in a humidity chamber at room temperature and rinsed in 0.1 M PBS. To identify cellular nuclei, tissues were then stained with 4,6-diamidino-2-phenylindole (DAPI) (Vector Labs, Burlingame, CA) separately before cover slipping.

2.6. Microscope spectral imaging for immunofluorescent quantification

Image acquisition for spectral analysis was preformed using Nuance spectral imaging system (http://www.cri-inc.com/products/nuancew.asp) [62], as described previously

[26,111]. Briefly, images of dorsal horn spinal cord were obtained using 20X objective with a Nikon TE-200 U inverted fluorescence microscope. Flat-field correction was applied in order to remove artifacts including uneven field illumination to produce a uniform illumination during image acquisition. A spectral library was then created using single-labeled control slides for each fluorophore and a label-free (autofluorescence) slide. The computed spectrum was then obtained by separating the known spectrum (autofluorescence) from mixed spectrum (single labeled) to produce pure labels of each fluorophore. This allowed for the un-mixing of multi-labeled slides to obtain composite images containing only the labels of interest. These composite images were then used for further analysis (see, Slidebook software image analysis). Sixteen spinal images per experimental group (2 adjacent sections plus 2 sections randomly separated by 140 μm totaling 4 sections per animal, with 4 animals per experimental condition) that were ipsilateral and contralateral to the sciatic manipulation were acquired and analyzed.

2.7. Slidebook software image analysis

Composite images were analyzed using Slidebook 6 software (Intelligent Imaging Innovations, Denver, CO). To eliminate signals originating from artifacts, an experimenter blinded to treatment groups determined an acceptable threshold of very low-level emission fluorescent intensity by closely replicating the composite computer image with that observed through the microscope eyepiece as described previously [26]. In addition, the dorsal horn of the spinal cord was outlined for analysis eliminating the surrounding white matter and peri-spinal blank space. The image was then refined to include the predetermined threshold within the outlined area. Analyses were conducted to include the ‘Sum Intensity’ (the total signal within the outlined dorsal horn) and ‘Area’ [total area within the outlined dorsal horn in micrometers squared (μm^2)]. ‘Fluorescence Intensity’ for the dorsal horn of the spinal cord was then calculated by dividing the ‘Sum Intensity’ by the ‘Area’. The average of four (2 adjacent and 2 randomly separated by 140μm sections) from a single slide was calculated to determine the value for each slide representing each individual animal. Each animal’s data were analyzed according to that detailed in Statistical Methods, below.

2.8. Spinal cord tissue digestion for flow cytometry

Following behavioral analysis conducted on Day 28 post-surgery, animals were deeply anesthetized (8–10 min, 5% vol. in oxygen). Peritoneal exudate cells (PECs), spleens and peripheral blood samples were collected (section 2.9) from rats followed by transcardial ice-cold 0.1M PBS (pH = 7.4) perfusion. With the body placed on ice, a laminectomy was performed and spinal cord L4-L6 was collected into RPMI 1640 media ((medium originally developed by Roswell Park Memorial Institute, purchased from Sigma-Aldrich, St. Louis, MO) that remained on ice until processing. Spinal tissues were digested according to the manufacturer’s instructions (Miltenyi gentleMACS™ protocol) for single-cell suspension of neural tissue. Briefly, spinal tissues were minced with fine tip scissors and digested at 37°C with collagenase/dispase (1mg/mL) (Roche Diagnostics, Indianapolis, IN) and deoxyribonuclease-1 (DNase-1, 10 mg/mL) (Sigma-Aldrich, St. Louis, MO). For optimal enzymatic digestion, tissue samples were incubated under slow, continuous rotation using a rotator. The gentleMACS Dissociator (Miltenyi Biotec, San Diego, CA) was used to dissociate the tissue between enzymatic incubation steps. Following digestion steps, cell

suspensions were passed through 70 μm followed by 40 μm cell strainers (Corning™ sterile cell strainers, Fisher Scientific, USA). Cells were incubated with magnetically labeled myelin removal beads (Miltenyi Biotec, San Diego, CA), washed and passed through MACS LS columns in conjunction with MACS Separator magnets (Miltenyi Biotec, San Diego, CA). The resultant eluent is both myelin-depleted and microglia/leukocyte-enriched.

2.9 Preparation of peripheral blood, peritoneal exudate cells (PECs) and spleen for flow cytometry

To collect immune cells from the peritoneal cavity, the ventral surface of anesthestized rats was shaved, cleaned with soapy water and sprayed with 70% ethanol. A small incision was made on skin with surgical blades and the underlying muscle was teased apart with blunt scissors followed by adding 30 ml Iscove's media (Sigma-Aldrich, St. Louis, MO) to the peritoneal cavity and massaged vigorously (with the incision clamped) for ~1.0 – 1.5 min, after which ~15–20 ml of peritoneal exudate cells (PEC) were collected and spun at 1200 RPM for 8 min. The resultant cell pellet was resuspended with 1 ml hypotonic salt solution (ACK lysis buffer; Sigma-Aldrich, St. Louis, MO) to lyse red blood cells (RBCs). Cells were incubated for 5 minutes on ice, washed twice and resuspended in ice-cold PBS. Cells were counted followed by viability dye staining (section 2.10). Spleens were harvested in RPMI and homogenized via passage through a 40μm cell strainer (BD Falcon™) to prepare a single cell suspension. RBCs were lysed similarly to that conducted with PECs and cells were washed and diluted with RPMI 1640 complete medium supplemented with 10% (v/v) fetal bovine serum (FBS) (Sigma), 2.0 mM L-glutamine (Thermos Fisher Scientific, PA, USA), 50 μM 2-mercaptoethanol (Sigma-Aldrich), 100 U/ml penicillin and 100 μg/ml streptomycin (Thermos Fisher Scientific, PA, USA) to a cell density of 1×10^6/ml for *in vitro* culture experiments described in section 2.11.

One ml peripheral blood was collected (in BD vacutainer^R K2EDTA blood collection tube) from deeply anesthetized animals through cardiac puncture immediately before transcardial perfusion. Peripheral blood mononuclear cells (PBMNs) were isolated using Ficol Premium 1.84 (GE Healthcare Life Sciences, PA, USA) according to the manufacturer's instructions. Briefly, 1 ml blood was diluted to 4 ml with PBS (w/o Ca/Mg) and layered on 3 ml Ficol in a 15 ml conical tube and centrifuged at 400×g for 30 min at 20°C, without brakes. PBMNs were collected from the interface and washed twice with PBS at 400×g for 10 min at 20°C. Cells were resuspended in PBS on ice until proceeding to viability dye staining (section 2.10).

2.10. Flow cytometry analysis for surface immune markers

Given that alpha-beta integrin heterodimers are required to mediate leukocyte trafficking, and leukocyte accumulation occurs in spinal tissue following peripheral neuropathy [22,30,38], microglial/macrophage activation and integrin expression were evaluated. Using the surface marker CD45 (protein tyrosine phosphatase C, also known as common leukocyte antigen) in combination with CD11b (also known as macrophage-1/Mac-1), we identified microglia and macrophages [33,95] and analyzed their CD11b fluorescent intensity separately. We also analyzed β_1 and β_2 integrin and MHC class II (MHC2) expression. MHC2 is typically expressed on antigen presenting cells (APCs) and upregulation of MHC2

is associated with activated APCs that are able to stimulate and activate myeloid and $CD4^+$T cells [68].

For flow cytometric analyses, live cells were counted on a hemocytometer using the trypan blue staining exclusion criteria. Cells were resuspended at 1×10^6/mL in PBS. Between 0.2×10^6 – 1×10^6 cells were transferred in a FACS tube (BD Falcon™, MA, USA) and pelleted by centrifugation at 300×g for 5 min at 4°C, with the supernatant discarded. Cells were then resuspended in PBS (without calcium and magnesium; Sigma-Aldrich, St. Louis, MO) and stained with Viability Dye eFluor® 450 (eBioscience, San Diego, CA) for 30 min, washed with FACS buffer (1x PBS containing 1.0% bovine serum albumin, and 1mM EDTA) and incubated with a saturating solution of Fc block (BD Biosciences, San Jose, CA, USA) for 10 min followed by staining with fluorochrome-conjugated antibodies for 30 min. All of these steps were conducted on ice. Antibodies against rat CD11b, LFA-1 (CD11a) (BD Biosciences San Jose, CA, USA), and rat CD45, MHC2 and CD29 (eBioscience, San Diego, CA, USA) were used for 0.125–0.5 ug/10^6 cells, as recommended by the manufacturer. Following antibody staining, cells were washed and resuspended in 250μl FACS buffer and then passed through a 40 μm cell strainer immediately prior to analysis to avoid cell clumping. At least 50,000 live cell events were collected for each sample. Data were acquired using the BD LSR Fortessa cell analyzer (BD Biosciences, San Jose, CA) and analyzed using FlowJo software v.8.7.4 (Treestar Inc., Ashland, USA). Live cells were identified based on their size, granularity (FSC vs SSC) and fluorescent viability dye staining. Microglia and macrophage were identified and their activation (CD11b expression levels) were assessed by examining the geometric mean fluorescent intensity (GMFI) analysis, which is the mean of logarithm values and represented as the antilog, as cell surface immunofluorescence data is logarithmically transformed to capture the wide ranging dynamic signals detected from biologically heterogeneous samples typically observed from flow cytometry sampling [37,74]. These data follow a lognormal distribution and GMFI is widely used for flow cytometry-acquired detection of cell surface receptors [14,90].

For β-integrins and MHC2 expression analysis, only live cells were gated on medium to high CD11b expression levels. Spinal/peripheral $CD11b^+$ cells (microglia and other leukocytes) were then plotted for LFA-1/CD29 or MHC2 expression as a function of CD11b expression. LFA-1^+, $CD29^+$ or $MHC2^+$ cells were identified based on isotype controls.

2.11 Intracellular detection of CCL2 by flow cytomtery

Splenocytes collected from each rat within each experimental condition were examined for CCL2 production upon stimulation. Splenic cells were cultured to detect intracellular CCL2 as described previously [18] with the following minor modifications. Splenocytes were plated in a 24-well culture plate (Corning Costar, Sigma-Aldrich), 1×10^6 cells/well and stimulated with PMA (a phorbol ester, Protein Kinase C activator, 50 ng/ml) and ionomycin (a calcium ionophore, 1ug/ml), incubated for 5 hours at 37°C and 5% CO_2. The combination of PMA/ionomycin is sufficient to activate many cell types including macrophages and T cells [32,44]. In order to block secretion of cytokines from activated splenic leukocytes, 2ul/ml protein transport inhibitor cocktail (containing brefildin A and monensin, from eBioscience) was simultaneously added with PMA/ionomycin solution at the beginning of

the cultures. Protein transport inhibitor cocktail inhibits the intracellular protein secretory/transport pathway resulting in the accumulation of secreted proteins in the lumen of the endoplasmic reticulum and in the Golgi apparatus which can be detected by intracellular staining and flow cytometric analysis [89]. Following 5hr of stimulation, splenic cells were gently removed from the wells, washed twice with PBS and stained with viability dye, CD45, and CD11b surface markers as described in section 2.8. Cells were fixed with 4% PFA (Sigma-Aldrich) for 10 min at room temperature, washed with FACS buffer and permeabilized with 0.3% saponin (Sigma-Aldrich) in FACs buffer followed by incubation with anti-rat CCL2 (eBioscience, San Diego, CA, USA) for 30 min on ice in the dark. Cells were then washed twice in saponin-FACs buffer and proceeded to flow cytometer data acquisition. Live $CD45^{+}CD11b^{+}$ cells were identified and proportions of $CCL2^{+}$ leukocytes were evaluated based on isotype control.

2.12. Tissue lysate preparation and multiplex determination of cytokine and chemokine expression

Flash frozen sciatic nerve and DRG tissue samples were kept on ice and homogenized using a Fisherbrand™ Disposable Pestle system (Fisher Scientific) with subsequent sonication (in a buffer with protease inhibitors according to the manufacturer's instructions. Tissue samples were centrifuged at 4,200×g, at 4°C for 10 min to pellet cellular debris. Cellular lysate protein concentrations were determined by Quickstart™ Bradford protein assay (BioRad, Hercules, CA, USA). Sciatic nerve cytokine expression levels were then determined using a V-PLEX™ immunoassay (MesoScale Discovery, Gaithersburg, MD, detailed below) panel for identification of the cytokines and chemokines: TNFα, IL-1β, IL-6, IL-10 and CXCL1, as previously validated [63,77]. IL-10 levels in L4-L6 DRGs were also measured using MesoScale Discovery immunoassay platform. All V-PLEX™ immunoassay assays were conducted according to manufacturer's instructions.

The V-PLEX™ immunoassay applies electrochemiluminescence technology to precisely measure protein concentrations of multiple cytokines simultaneously with high sensitivity and reproducibility. Tissue lysates (100 μg total protein) from experimental tissue samples or calibrator (provided in the kit) were loaded onto a 'multi-spot' plate. Each well in the plate is pre-coated with capture antibodies on independent and well-defined spots. Analytes in the tissue sample were then bound to capture antibodies attached to the working electrode surface. Immobilized proteins were then incubated with detection antibodies conjugated with electrochemiluminescent labels (MSD SULFO-TAG™). A Quickplex SQ 120 Imager (MesoScale Discovery, Gaithersburg, MD) was used to read the plate via application of an electrical current to the plate electrodes and subsequent measurement of light intensity emitted by SULFO-TAG labeling. This provided a quantitative measure of sample analytes. Samples were run in duplicate and the coefficient of variation was less than 15% for all analytes.

2.13. Statistical analysis

All behavioral data of hindpaw threshold responses were analyzed by SPSS (IBM, Chicago, IL, USA). At BL, a 2-way analysis of variance (ANOVA) for between-subject factors of prenatal exposure (Sac versus PAE) x surgical manipulation (sham versus CCI) was

analyzed. Based on previous data showing strong correlations between repeated measurements, it was estimated that the planned sample size for squad 3 would be sufficient to detect effects that account for as little as 4% of the observed variance, with 80% power and traditional α=0.05. Data from microscope-acquired images reflecting immunoreactivity, flow cytometry, and protein V-PLEX™ immunoassays were analyzed using two-way ANOVA with GraphPad Prism version 6 software (GraphPad Software Inc., San Diego, CA, USA). To control the type I error rate during multiple comparisons, reported with adjusted P values, Fisher's LSD test was applied for post hoc examination of possible group differences. Groups were compared, *a priori*, between Sac + sham versus PAE + sham and PAE + CCI because we hypothesized that with some immune endpoints, PAE without CCI alters immune cell phenotype. The threshold for statistical significance was set *a priori* at α = 0.05 for all sets of multiple comparisons. In all cases, the data are presented as the mean ± SEM.

3. Results

3.1. Voluntary maternal drinking paradigm

Long-Evans rat dams consumed an average of 2.04 ± 0.10 g/kg/day of ethanol throughout gestation. This level of drinking produced a peak serum ethanol concentration of 60.8 + 5.8 mg/dL. This voluntary drinking paradigm did not affect maternal weight gain, litter size, offspring birth weight or growth curves (data not shown, see [83]).

3.2. PAE potentiates CCI-induced allodynia

Light mechanical touch assessed at BL revealed similar levels of hindpaw sensory threshold responses between all groups (Fig 1a–b). These BL values reveal that PAE in the absence of peripheral injury or challenge does not produce overt sensitivity to light touch suggesting that the deleterious effects of PAE are unmasked following challenge. Indeed, while all rats resumed normal activity (active grooming, weight gain) within one day of either CCI or sham surgery, clear development of bilateral allodynia (Fig 1a–b) assessed on Days 3 and 10 after surgery (N=10 rats/group) occurred in Sac-treated CCI-operated rats with the most dramatic responses observed in PAE-CCI rats compared to sham-treated controls (Fig 1a–b). It is important to point out that the enhanced allodynia observed in PAE-CCI rats was ~10-fold greater than Sac-CCI rats. Moreover, enhanced allodynia on Day 3 from the contralateral hindpaw of PAE-CCI rats (Fig 1b) strongly support that pathological processing is occurring at the level of the spinal cord where allodynia signaling develops. Accordingly, enhanced allodynia in PAE-CCI rats may be driven by aberrant immune responses not only in the damaged sciatic nerve, but also in the DRG where light touch neurons send their axons to the spinal cord. These data are the first demonstration that moderate PAE markedly exacerbates allodynia in adult offspring, as assessed using a standard model of peripheral neuropathy.

3.3. PAE potentiates spinal glial activation in rats with enhanced allodynia

As noted previously, glial activation in the CNS is a common characteristic between animal models of PAE and models of chronic neuropathy that produces allodynia. Here, potentiated spinal glial activation was evaluated in PAE rats with CCI-induced allodynia. No differences

between cryoprotected and paraffin-embedded spinal cord processing were observed with regard to the pattern of GFAP immunoreactivity (IR) between each treatment group. Representative photomicrographs of paraffin-processed GFAP IR spinal cords and the corresponding image analysis are shown in supplemental figure 1A and B. Representative photomicrographs of cryosectioned spinal cords from squad 2 show GFAP IR, demonstrating augmented spinal cord astrocyte activation occurs in the dorsal horn from behaviorally verified rats are shown (Fig 2a). Analyzed GFAP IR revealed a trend toward increased bilateral astrocyte activation from the Sac-treated rats with CCI compared to the Sac-treated sham-operated group (Fig 2b). However, while sham-operated PAE-rats reveal slightly increased GFAP IR compared to Sac-sham, the largest increase in GFAP IR is observed in PAE rats with CCI.

During the image acquisition and analysis of Iba1 IR from paraffin processed tissue, it was determined that extended decalcification results in complete loss of Iba1 signal resulting in reduced spinal cord samples per experimental condition (Sac + sham N=4, Sac + CCI N=5, PAE + sham N=4, and PAE + CCI N=5). Thus, reliable Iba1 IR data from decalcification procedures of spinal cords was not possible. However, non-decalcified cryosectioned spinal cords revealed microglial activation as assessed by Iba-1 IR, is increased following peripheral neuropathy (Fig 2c–d). However, the greatest Iba-1 IR is observed in spinal cords from PAE-CCI rats, both ipsilateral and contralateral to CCI. Representative ipsilateral photomicrographs of microglial analysis are shown Fig 2c. Importantly, macrophages cannot be ruled out, as Iba-1 is also detected in macrophages, which may contribute to the overall increases in Iba-1 IR. The data show that both astrocytes and microglial activation markers are significantly potentiated in PAE rats following standard peripheral nerve CCI damage. These data suggest primed spinal glia may result as a consequence of PAE that contributes to heightened allodynia in rats.

3.4 PAE-associated increases in allodynia persist for at least four weeks

One possibility observed from PAE-induced potentiated allodynia could be that these heightened sensory responses are transient, with resolution of allodynia occurring shortly after Day 10 following CCI. That is, compensatory spinal glial anti-inflammatory signaling factors may act to resolve heightened glial reactivity with concurrent resolution of exaggerated allodynia to typical levels frequently observed from CCI. Enduring potentiated allodynia can be readily addressed given typical levels of allodynia following CCI are well-characterized and known to persist for 70–90 days prior to spontaneous reversal [26,92]. Therefore, to examine whether PAE potentiates persistent allodynia, a separate group of rats were evaluated for allodynia over a 28-day time-course, which evidence shows is long before spontaneous resolution of allodynia occurs. All groups of rats revealed normal hindpaw response thresholds at BL (Fig 3). However, due to spontaneous death (a Sac-treated rat before surgery) or the presence of ipsilateral hindpaw autotomy (N=2 in PAE + CCI and N=1 in Sac + CCI treatment group), some rats were eliminated. Typically <1% of experimental rats reveal hindpaw autotomy in our laboratory. As with squad 1 and 2 shown in Figure 1, following sham surgery, Sac- and PAE- treated rats remained stably responsive with hindpaw response thresholds consistently similar to pretreatment BL values throughout the 28-day time-course. Conversely, Sac-treated controls with CCI revealed a clear increase

in hindpaw sensitivity, as paw withdrawal responses stably occur at <1 g touch stimuli, as predicted. However, PAE with CCI revealed the most robust bilateral increase in hindpaw sensitivity, with paw withdrawal responses occurring ~0.03 g beginning on Day 3 and continuing throughout the entire 28-day time-course (Fig 3). These data reveal that adult onset potentiated allodynia from PAE endures for an extended period with no evidence of resolution for 28 days.

3.5. PAE alters lumbar spinal immune cell activation in rats with adult-onset CCI-allodynia

Astrocytes and microglia are not the only cell populations strongly implicated in spinal immune signaling that underlie chronic neuropathy. Leukocytes (e.g. macrophages, neutrophils, T cells, and dendritic cells) trafficking to the spinal cord following peripheral nerve damage are also gaining recognition as key contributors in the pathogenesis of chronic neuropathic pain. To address this possibility, lumber spinal cords from behaviorally verified rats (behavior shown in Fig 3) were analyzed by flow cytometry to distinguish resident microglia ($CD11b^{high}CD45^{low\text{-}medium}$) and macrophage ($CD11b^{high}CD45^{high}$) populations. We first examined overall spinal cell accumulation and observed the greatest spinal cell counts occurred in PAE rats with CCI compared to either Sac-treated groups or sham-operated PAE rats (Fig. 4a). While our data reveal no significant differences in the proportion of microglia and macrophage populations between experimental conditions (data not shown), CD11b fluorescent intensity is upregulated on both microglia (Fig 4b) and macrophages (Fig 4c) following neuropathy, with the most robust upregulation occurring in spinal cords of PAE rats. These data suggest that as a consequence of PAE, spinal microglia and macrophages are primed to over-respond as observed by enhanced activation (CD11b intensity).

3.6. PAE alters integrin and MHC class II expression on immune cells

As previously noted, critical adhesion molecules that allow for peripheral immune cell trafficking include the β_2-integrins Mac-1 (CD11b/CD18) and LFA-1 (CD11a/CD18), and the β_1-integrin VLα4 (CD49d/CD29). Given the augmented macrophage and microglial activation observed in the spinal cords of PAE rats, an examination of enhanced peripheral immune cell activity that leads to elevated β-integrin activation and expression was assessed by first measuring CCL2 expression on stimulated splenocytes (a.k.a. peripheral leukocytes). CCL2 co-expressed with β-integrins promotes activated β-integrin and integrin-mediated leukocyte migration [30,61]. We reasoned PAE may enhance leukocyte responses that include elevated CCL2 production following immune cell stimulation. Given CCL2 signaling is critical for β_2 - integrin adhesion molecule activation, CCL2 on peripheral immune cells may be a critical factor potentiating leukocyte homing to the glial- and cytokine-activated spinal cord. In support of this possibility, stimulated splenic cells *in vitro* collected from Sac-Sham, Sac-CCI, PAE-Sham and PAE-CCI revealed CCL2 expression is greatest from PAE-CCI neuropathic rats (Fig 5a). These data support the possibility that elevated CCL2 increases LFA-1 on immune cells with concurrent activated LFA-1 conformation thereby facilitating immune cell migration.

Given the peritoneal cavity is a region routinely enriched with trafficking myeloid cells that migrate from the primary immune organs, PAE-induced elevated β_2-integrin expression was

examined in leukocytes collected from peritoneum. Expression of LFA-1 on $CD11b^+$ PECs is greatest from PAE-treated rats with CCI compared to either PAE-Sham or Sac-CCI and PAE-Sham rats (Fig. 5b), supporting the possibility that PAE leads to functional consequences of peripheral immune cell reactivity. Moreover, in an exploratory experiment examining lumbar spinal cord, a subset of rats from each treatment condition (animal numbers were restricted by the availability of surface antigen markers at the time of spinal dissection) revealed a similar pattern of elevated $CD11b^+$/LFA-1^+ cells between groups (Fig. 5c), with the greatest increase of $CD11b^+$/LFA-1^+ cells observed from spinal cords of PAE-CCI rats compared to all other groups.

As with β_2-integrins (i.e. LFA-1), the β_1-integrin adhesion molecules play an additionally important role in peripheral leukocyte trafficking, which is supported by the current data demonstrating elevated $CD29^+$ (maker for β_1-integrins) myeloid cells, as identified by CD11b, are present in spinal cords of Sac rats with chronic CCI neuropathy as well as in PAE rats without (PAE-Sham) or with (PAE-CCI) neuropathy (Fig. 5d). These data are striking in that PAE alone is sufficient to alter β_1-integrin expression profiles in the spinal cord, in further support that PAE alters some aspects of immune cell activation under basal conditions. Representative flow cytometry plots and quantification of β2 integrin and LFA-1 (activated and inactivated) expressing $CD11b^+$ (predominantly macrophage/microglia) cell populations in the lumber spinal cord revealed PAE rats have more integrin expression than Sac-treated controls (Fig 5e–f). Interestingly, LFA-1 did not increase on myeloid cells identified in PBMNs (data not shown), indicating differentiated mature tissue macrophages had already migrated to the inflamed tissue [46].

The possibility that elevated basal immune cell activation occurs as a consequence of PAE was further explored in tissues from the same subset of rats examined for β-integrins. Flow cytometric analyses revealed PAE-sham significantly contributes to an increase in lumbar spinal cord $MHC2^+$ cells compared to Sac-treated shams (Fig 5g). Comparable MHC2 expression levels were observed in cells from Sac-treated CCI animals and PAE with (PAE-CCI) or without (PAE-Sham) neuropathy. Specifically, lumbar spinal cell populations with $MHC2^+CD11b^+$ cell surface expression revealed an average percent increase from 30±1.2 (Sac-Sham) to 38±2.7 (Sac-CCI), or to 43.5±2 (PAE-CCI) at day 28 post CCI. Combined, the increased spinal MHC2 and β-integrin expression in PAE-CCI rats is indicative of an enhanced proinflammatory microenvironment in the lumber dorsal horn.

Integrin expression levels may further point to ongoing activation and migration of $CD11b^+$ leukocytes with augmented MHC2 expression, as analysis of cells revealed that the most profound increases in $CD11b^+MHC2^+$ PBMNs (Fig 5h) and PECs (Fig 5i) occurs in PAE-CCI neuropathic rats. It is important to point out that no significant alterations in $CD29^+$/$CD11b^+$ cells from PBMNs or PECs (data not shown) were observed, suggesting that increases in CD29 in lumbar $Cd11b^+$ cells indicate microglial-specific regulation by PAE.

3.7. Increased pro-inflammatory cytokines in sciatic nerve of PAE rats with CCI-induced allodynia

Little is understood about the effects of PAE on peripheral immune cell function. Enhanced allodynia observed in PAE animals may also be due to pathological activation of peripheral

immune cells recruited to the sciatic nerve injury site. Indeed, compared to Sac or PAE sham controls, ipsilateral sciatic nerves from Sac-treated rats with chronic allodynia revealed substantially elevated IL-1β (Fig 6a), IL-6 (Fig 6b), TNFα (Fig 6c) and CXCL1 (chemokine C-X-C ligand 1 (a neutrophil chemoattractant, Fig 6d) protein expression. Moreover, a potentiated and significant increase of IL-1β, IL-6 and TNFα protein was observed in nerves from PAE rats with chronic neuropathy (CCI-PAE) (Fig 6), suggesting *in utero* alcohol exposure primes proinflammatory peripheral immune cell reactivity that may underlie these observations. While a slight trend toward increased CXCL1 levels in sciatic nerves from PAE with CCI (Fig 6d) was observed, these changes were not statistically significant. Robust allodynia observed in PAE-CCI that occurs in parallel with enhanced sciatic nerve IL-1β, IL-6 and TNF-α but not CXCL1, suggests the actions of CXCL1 at the sciatic nerve by peripheral immune cells are less critical in mediating PAE-potentiated allodynia. However, these data are the first demonstration that peripheral neuropathy from sciatic nerve CCI generates substantially elevated CXCL1 in the ipsilateral sciatic nerve examined 28 days after injury. Importantly, examination of the contralateral sciatic nerve did not reveal increased cytokine and chemokine protein levels compared to Sac-treated sham controls (data not shown), which validates that CCI is a highly localized model of discrete unilateral sciatic nerve damage despite observing chronic bilateral allodynia.

3.8. Dysregulation of IL-10 protein in the DRG and the sciatic nerve of adult PAE rats following CCI

The current data reveal a robust PAE-induced increase in proinflammatory immune cytokines is present in the ipsilateral sciatic nerve. Given the observation of increased proinflammatory cytokines, the anti-inflammatory cytokine IL-10 was examined to investigate the compensatory effects in neuropathic PAE rats. The current data demonstrate that compared to IL-10 levels in the DRG from Sac-treated sham rats, Sac-treated CCI rats show decreased IL-10 levels commensurate with ongoing allodynia in these rats. Unexpectedly, sham-operated PAE rats revealed a down-regulation of IL-10 compared to Sac-treated sham rats (Fig. 7a), suggesting PAE creates pathological susceptibility to proinflammatory immune responses. Indeed, the greatest IL-10 DRG decrease is observed in PAE rats with chronic CCI-induced potentiated allodynia (Fig 7a).

The ipsilateral peripheral nerve axon reveals a different IL-10 profile of expression. A compensatory IL-10 protein increase occurs in Sac–CCI rats compared to Sac and PAE sham-treated rats (Fig. 7b). Conversely, this compensatory increase in the ipsilateral sciatic nerve of PAE rats with CCI is completely absent, suggesting that the peripheral immune signals required for typical anti-inflammatory responses at the axon following injury are dysregulated.

4. Discussion

Increasing evidence indicates that PAE creates long-lasting alterations to immune function. A number of studies using animal models of PAE show brain region-specific microglial and astrocyte activation and elevated proinflammatory cytokines [3,27,53,102,103]. Here, we extended observations of PAE on immune function and focused specifically on the effects of

PAE on adult-onset neuropathic pain with concurrent changes in spinal glial and immune cell markers as well as cytokine levels in the nociceptive system. We provide new insights that PAE potentiates bilateral allodynia of both short and long duration (Fig 1 and 3) in adult rats with sciatic nerve damage. Importantly, these behavioral changes in allodynia are not a short-term transient observation. Astrocytes and microglia in the dorsal horn of the spinal cord from neuropathic rats reveal PAE augments their functional activation as assessed by microscopic analysis (Fig 2 & Supplementary Fig 1). Immunohistochemical evaluation is further supported by flow cytometric analysis revealing the activation profile of microglial and macrophage cell populations is dramatically up-regulated in neuropathic PAE rats (Fig 4). The elevated lumbar spinal immune cell activity is further supported by increased MHCII, and integrin expressing $CD11b^{+}$ microglia and leukocytes in the spinal cord and in the periphery (Fig 5). In line with these observations, analysis of the ipsilateral sciatic nerve and DRG reveal PAE treatment in combination with neuropathy results in increased protein expression of IL-1β, TNF-α and IL-6 (Fig 6) with a simultaneous suppression of sciatic nerve and DRG IL-10 (Fig 7). Together, these data provide evidence that PAE generates consistent and potentially life-long spinal and PNS glial and immune cell hyper-reactivity to a second insult produced by a localized sciatic nerve trauma initiated in adulthood.

4.1. PAE- primed glial activation

PAE may lead to heightened and enduring glial reactivity (brain and/or spinal cord) throughout adulthood leading to aberrant neuroimmune signaling [100]. Our data suggest moderate PAE primes spinal microglia and astrocytes such that the response of these cells to subsequent “damaged self” signals that occur during Wallerian degeneration from peripheral nerve damage is exaggerated. Previous studies show microglial proliferation and long lasting microglial reactivity from non-PAE animals with peripheral nerve injury, as evidenced by increased CD11b and Iba-1 immunoreactivity [39,54], which is also expressed on monocytes/macrophages. Data in the current study reveal PAE-induced heightened microglial reactivity is distinguished from the observed heightened monocytes/macrophage reactivity using flow cytometric analysis [33,91]. Specifically, under CCI-induced pathological conditions, a ~13% increase in CD11b intensity on microglia occurs, whereas a 36% increase in CD11b intensity on monocytes/macrophages is observed in PAE compared with Sac rats. However, the processes underlying the effects of PAE per se on immune function may be better ascertained by examining basal levels of anti-inflammatory cytokines such as IL-10 in the anatomically nociceptive-relevant DRG. Indeed, DRG IL-10 protein levels from PAE rats with sham treatment are remarkably suppressed compared to their Sac-treated counterparts. Importantly, prior reports demonstrate DRG IL-10 protein levels are significantly greater in sham-treated healthy controls compared to those rats with allodynia from CCI [110,111]. These prior reports show satellite glia are a cellular source of DRG IL-10. Thus, the current data in light of these prior reports suggest PAE blunts the protective actions of basal DRG glial-derived IL-10 against the development of augmented proinflammatory glial actions and resultant allodynia.

Microglia and leukocyte activation is often correlated to their integrin and MHC expression. In fact, expression of β-integrin and MHC molecules on microglia are regulated by pro- and anti-inflammatory cytokines present in the microenvironment [66]. CCI upregulates

endothelial adhesion molecules such as platelet endothelial cell adhesion molecule 1 (PECAM-1) and intercellular cell adhesion molecule 1 (ICAM-1) [97]. These adhesion molecules facilitate migration of T cells and monocytes/macrophages expressing integrins and possibly reinforce immune cell actions. Spinal MHC expression is important in generating neuropathic pain, suggesting the crucial role of antigen presenting cells' engagement with $CD4^+$ T cells [97]. Our data suggest PAE, with or without neuropathy, increased LFA-1^+, $CD29^+$ and $MHC2^+$ microglia and leukocytes in the lumbar spinal cord, which is further indicative of PAE-induced priming of spinal immune cells. Further studies are needed to determine whether PAE-induced priming leads to increased activation of integrin on leukocytes [7] possibly driven by increased CCL2-mediated interactions, as previously observed in the brain of PAE offspring [28].

While the mechanisms underlying immune activation and potentiated neuropathic pain as a consequence of alcohol exposure are unknown, prior work has demonstrated a possible immune-mediated link. A previous report suggests that in adult animals, ethanol treatment alone can induce microglial activation and neuropathic pain-like symptoms [69]. *In vitro* and *in vivo* studies support direct and indirect alcohol-mediated activation of the innate immune receptors, Toll-like Receptor (TLRs) and NOD-like receptors (inflammosome NLRs) [3,4,67]. Chronic ethanol treatment (87–140 mg/dl) in adult female mice can activate TLR4 signaling on glial cells, inducing the production of pro-inflammatory molecules and upregulating CD11b and GFAP [3]. Microglia from alcohol treated mice increase neuronal apoptosis in TLR4-dependent pathways [31]. However, how in utero alcohol exposure affects neuroimmmune functions in the adult brain remains speculative. Recent literature suggests that PAE alters CNS fetal programming and increases later life vulnerability to stress, depression and anxiety disorders [45]. Even a low level immune activation produces cognitive deficits in PAE animals [100]. In addition, moderate PAE rats display exaggerated immune responses in later-life as a consequence of low level of immune activation [100]. Interestingly, this study reported that the effect of low level of alcohol exposure to the maternal immune system is limited or undetectable. However, placenta or fetal brain is far more responsive to the detrimental effects of alcohol. Even low levels of alcohol exposure during early embryonic development regulate gene expression of many pro- and anti-inflammatory molecules in both the fetal brain and the placenta. These observations additionally reveal sex-specific differences in some cytokine and cytokine genes. The authors speculate that because microglia in the developing brain are particularly sensitive to small disturbances and act as crucial regulators in many neurodevelopmental processes such as cell proliferation, dendritic spine pruning and apoptotic cell clearance [6,24,95], alcohol induced activation of microglia during specific developmental stages can have significant consequences for long-term neural function.

Consistent with our observations, another study reported possible alcohol related priming in splenic cells in adulthood, despite in utero alcohol exposure occurred before spleens had developed. Additionally, emerging evidence of epigenetic changes due to prenatal alcohol exposure has been reported [57]. For example, distinct DNA methylation patterns observed in adolescents and children with FASD [73] may effect immune organ development and immune-related gene expressions.

Another possible mechanism for moderate PAE-induced glial priming could be via an altered spinal-blood barrier. Curiously, one report demonstrated that PAE rat offspring whose mothers achieved average serum ethanol concentrations of 140 mh/dL (~0.14 gm/dl) revealed altered morphological development of the glia limitans, a structure consisting of astrocyte endfeet in contact with the pia mater and with capillary endothelial cells [59]. In a separate study, PAE (0.09gm/dl) upregulated the vascular factor, vascular cellular adhesion molecule 1 (VCAM-1) in the brain [27]. Thus, while speculative, PAE may cause "leakiness" in the neurovascular barrier leading to chronic low-level glial reactivity, which may facilitate CNS leukocyte trafficking following subsequent challenges such as peripheral nerve damage. Our observation that CCI increased viable cell counts in the spinal cord with the greatest increase in PAE-CCI animals suggests a potential increase in leukocyte infiltration in PAE rats with chronic allodynia. Future studies examining other spinal cord infiltrating leukocyte subsets (e.g. neutrophils and T cells) will provide insight into other contributing factors leading to potentiated allodynia as a consequence of peripheral nerve injury in PAE rats.

4.2. PAE affects peripheral immune cell function

In peripheral nerve injury, cytokines and chemokines produced at the injured site are important components influencing central pain processing [65,88]. In the current report, analysis of the ipsilateral sciatic nerve reveals IL-1β, IL-6, TNFα and the chemokine CXCL1 levels are increased in all chronic allodynic rats, in support of prior reports showing that these cytokines at the sciatic nerve strongly contribute in neuropathic pain [54,88]. However, the current report extends these findings by showing PAE potentiates IL-1β, IL-6 and TNFα in chronic allodynic rats. While essential in spinal pain processing [16,113], levels of sciatic nerve CXCL1 in neuropathic rats are similar between Sac and PAE treated groups despite the potentiated allodynia observed in PAE rats.

Consistent with another report suggesting increased IL-10 mRNA in the endoneurium of the transected rat sciatic nerve [98], we have observed an increase in IL-10 in the ipsilateral sciatic nerve of chronic allodynic animals. This expected sciatic nerve IL-10 rebound observed in Sac rats with neuropathy was completely absent in PAE rats with neuropathy, suggesting a lack of control over the damaging effects of the proinflammatory immune cell response around the nerve that likely leads to further nerve damage.

The data from the current study suggests that PAE-related glial cell priming extends beyond glial cells and includes alterations in peripheral immune cell function. Indeed a recent study showed that moderate PAE leads to exaggerated expression of pro-inflammatory cytokines in the embryonic brain and also in the adult spleen in response to peripheral lipopolysaccharide (LPS) challenge in adulthood [100]. Here, we significantly extend these findings and report PAE-augmented MHC2 and LFA-1 expression on peripheral immune cells with a heightened ability to produce chemo attractants or inflammatory cytokines such as CCL2. In addition, we found that inflammatory responses in PAE animals in their adulthood correlate with a deficiency in IL-10 at the sciatic nerve and DRG following peripheral nerve injury. Major cellular sources of IL-10 are macrophages and T-cells (mainly T-helper 1/Th1 and regulatory T/Treg) [51,82] that infiltrate the sciatic nerve and DRG

following CCI [88]. Interestingly, a number of studies show PAE alters cell-mediated immune responsiveness, as demonstrated by reduced proliferative responses of splenic or thymic T-cells [40,41,76,101]. However, this effect varied on the timing and extent of ethanol exposure [10,70,76]. Another study reported that T-cells from PAE animals show diminished responsiveness to IL-2, a critical cytokine known to augment T cell function. Thus, IL-2/IL-2R (IL-2 receptor) interaction may be interrupted leading to suppressed T-cell proliferation in PAE offspring [19]. It is noteworthy that IL-2 signaling is also essential for Th1 and Treg differentiation and function, and IL-2 primes Tregs to produce IL-10 upon secondary stimulation [25,60]. Together, these reports suggest IL-10 production by T-cells may be compromised in adult PAE rats, a notion that requires further confirmation.

There is growing body of evidence indicating there are sex-specific outcomes of PAE. Sexually dimorphic effects of hyper-responsive hypothalamic-pituitary- adrenal (HPA) activity in PAE offspring have been observed [109]. In fact, while the immediate inflammatory effects of PAE on placental cytokines are similar, the levels of these inflammatory factors are distinctly different in male versus female fetuses [100]. Neuroimmune sex differences extend beyond observations related to HPA axis hypersensitivity and have been observed in the spinal cord leading to neuropathic pain. Indeed, a recent report suggests spinal neuroimmune mechanisms leading to allodynia are distinctly different between male and female rodent animal models of peripheral neuropathy despite that pathological pain develops to the same magnitude and duration between the two sexes [93]. For example, the action of spinal T cells may dominate the events that lead to allodynia in female rodent subjects [93]. While prior reports demonstrate a functional T cell role in mediating pain after peripheral nerve injury occurs in males [8,17,22,39,54,88], it is the microglia/monocytes suspected to be key drivers over T cells in male mice/rats models.

While speculative, PAE-exposed females may be more susceptible to T-cell driven neuropathic pain. The augmented pro-inflammatory cytokines and deficiency in IL-10 observed in response to peripheral nerve injury may reflect exaggerated/dysregulated T-cell function in PAE animals, as IL-10 is a key regulatory cytokine produced by T-cells to suppress pro-inflammatory responses or immunopathology (for review [23]). LFA-1 and CD11b expression on T-cells have been shown to have functional importance for T-cell activation and T-cell differentiation to Treg or T-helper 17/TH17 T cells [105,106,108]. LFA-1 is also crucial for Th17 lymphocyte migration into the CNS [80]. Therefore, it is possible that PAE also alters LFA-1 and CD11b expression on T cells thereby altering T-cell function and migration to the CNS. Although the current report does not address the spinal action of other immune cells in males vs. females, the current findings provide a framework for future studies to address whether T-cell actions that traffic to the spinal and DRG regions are altered by PAE and thereby exacerbating allodynia. Specifically, a close examination of T-cell-specific cytokines such as IL-17A, which enhances IL-1 and TNF-α release from macrophages [52,96] may reveal a unanticipated mechanism by which PAE potentiates allodynia in females with CCI-induced neuropathy while remaining unaltered in males. Moreover, IL-23 and IL-15 that regulate IL-17 [56] can be examined to understand the local cellular cytokine/chemokine milieu.

A key finding in the current report is the observation of bilateral allodynia despite localized ipsilateral sciatic nerve damage. These behavioral observations strongly suggest that key pathological changes are occurring in the spinal cord because no proinflammatory cytokine changes were observed in the contralateral sciatic nerve or DRGs. Mirror pain (mechanical hypersensitivity on the uninjured mirror-image side of the body) has been reported clinically and observed in various animal pain models (for review [47]). In animal models, the pathogenesis of mirror image allodynia likely involves activated astroglial networks that communicate by gap-junctions to more distant sites such as the contralateral spinal cord, thereby affecting deeper lamina 5 wide dynamic range projection neurons. Evidence exists that spinal-glial activation; glial–neuronal interactions and extensive gap junctional connectivity of spinal glia contribute to contralateral neuropathic pain [50,94]. Moreover, released inmmunomodulatory cytokines can also be transported via the cerebrospinal fluid [64] to the contralateral spinal cord. In support of these possibilities, increased inflammatory cytokine expressions in the contralateral spinal cord have been detected that displays a cyclic pattern and often for a brief time course at a smaller magnitude than the ipsilateral side of injury [55,58,81,98].

4.3. Conclusions

We provide compelling evidence that moderate PAE potentiates adult-onset chronic allodynia. Additionally, PAE primes spinal glial and immune cells. In these same PAE rats, a robust decrease in anti-inflammatory cytokine IL-10 protein at the sciatic nerve lesion site and corresponding lumber DRGs occurs with a simultaneous increase in sciatic nerve proinflammatory IL-1β, IL-6 and TNF-α. These data indicate that PAE shifts the neuroimmune response towards proinflammatory properties and augments glial cell function to injury. Further, the current report shows PAE exerts significant and long-lasting effects on innate and possibly adaptive immunity that may induce susceptibility to chronic CNS pathological conditions such as neuropathic pain. These observations highlight how physiological adaptations of the fetus in response to adverse *in utero* conditions such as alcohol exposure may lead to long-term consequences of altered neuroimmune responses to subsequent immune challenges in their adulthood. These data also highlight potential contributing factors underlying why some individuals are more prone to develop chronic neuropathic pain than others [48].

Supplementary Material

Refer to Web version on PubMed Central for supplementary material.

Acknowledgments

We sincerely thank Becky J Lee, Genevieve Kate Phillips and Dr. Michael L Paffett at University of New Mexico Cancer Research and Treatment Center microscope facility for their critical guidance and assistance in microscope spectral imaging.

This work was supported by National Institute of Health grants AA023051, AA022534, DA018156 and AA014127 and dedicated Health Research funds from the University of New Mexico School of Medicine.

References

1. Ahluwalia B, Wesley B, Adeyiga O, Smith DM, Da-Silva A, Rajguru S. Alcohol modulates cytokine secretion and synthesis in human fetus: an in vivo and in vitro study. Alcohol. 2000; 21(3):207–213. [PubMed: 11091023]
2. Akers KG, Kushner SA, Leslie AT, Clarke L, van der Kooy D, Lerch JP, Frankland PW. Fetal alcohol exposure leads to abnormal olfactory bulb development and impaired odor discrimination in adult mice. Mol Brain. 2011; 4:29. [PubMed: 21736737]
3. Alfonso-Loeches S, Pascual-Lucas M, Blanco AM, Sanchez-Vera I, Guerri C. Pivotal role of TLR4 receptors in alcohol-induced neuroinflammation and brain damage. J Neurosci. 2010; 30(24):8285–8295. [PubMed: 20554880]
4. Alfonso-Loeches S, Urena-Peralta J, Morillo-Bargues MJ, Gomez-Pinedo U, Guerri C. Ethanol-Induced TLR4/NLRP3 Neuroinflammatory Response in Microglial Cells Promotes Leukocyte Infiltration Across the BBB. Neurochem Res. 2016; 41(1–2):193–209. [PubMed: 26555554]
5. Allan AM, Chynoweth J, Tyler LA, Caldwell KK. A mouse model of prenatal ethanol exposure using a voluntary drinking paradigm. Alcohol Clin Exp Res. 2003; 27(12):2009–2016. [PubMed: 14691390]
6. Antony JM, Paquin A, Nutt SL, Kaplan DR, Miller FD. Endogenous microglia regulate development of embryonic cortical precursor cells. J Neurosci Res. 2011; 89(3):286–298. [PubMed: 21259316]
7. Ashida N, Arai H, Yamasaki M, Kita T. Distinct signaling pathways for MCP-1-dependent integrin activation and chemotaxis. J Biol Chem. 2001; 276(19):16555–16560. [PubMed: 11278464]
8. Austin PJ, Kim CF, Perera CJ, Moalem-Taylor G. Regulatory T cells attenuate neuropathic pain following peripheral nerve injury and experimental autoimmune neuritis. Pain. 2012; 153(9):1916–1931. [PubMed: 22789131]
9. Baranek GT, Berkson G. Tactile defensiveness in children with developmental disabilities: responsiveness and habituation. J Autism Dev Disord. 1994; 24(4):457–471. [PubMed: 7961330]
10. Basham KB, Whitmore SP, Adcock AF, Basta PV. Chronic and acute prenatal and postnatal ethanol exposure on lymphocyte subsets from offspring thymic, splenic, and intestinal intraepithelial sources. Alcohol Clin Exp Res. 1998; 22(7):1501–1508. [PubMed: 9802535]
11. Bennett GJ, Xie YK. A peripheral mononeuropathy in rat that produces disorders of pain sensation like those seen in man. Pain. 1988; 33(1):87–107. [PubMed: 2837713]
12. Bodnar TS, Hill LA, Weinberg J. Evidence for an immune signature of prenatal alcohol exposure in female rats. Brain Behav Immun. 2016; 58:130–141. [PubMed: 27263429]
13. Boha R, Molnar M, Gaal ZA, Czigler B, Rona K, Kass K, Klausz G. The acute effect of low-dose alcohol on working memory during mental arithmetic: I. Behavioral measures and EEG theta band spectral characteristics. Int J Psychophysiol. 2009; 73(2):133–137. [PubMed: 19414050]
14. Bortell N, Morsey B, Basova L, Fox HS, Marcondes MC. Phenotypic changes in the brain of SIV-infected macaques exposed to methamphetamine parallel macrophage activation patterns induced by the common gamma-chain cytokine system. Front Microbiol. 2015; 6:900. [PubMed: 26441851]
15. Brady ML, Allan AM, Caldwell KK. A limited access mouse model of prenatal alcohol exposure that produces long-lasting deficits in hippocampal-dependent learning and memory. Alcohol Clin Exp Res. 2012; 36(3):457–466. [PubMed: 21933200]
16. Cao DL, Zhang ZJ, Xie RG, Jiang BC, Ji RR, Gao YJ. Chemokine CXCL1 enhances inflammatory pain and increases NMDA receptor activity and COX-2 expression in spinal cord neurons via activation of CXCR2. Exp Neurol. 2014; 261:328–336. [PubMed: 24852102]
17. Cao L, DeLeo JA. CNS-infiltrating CD4+ T lymphocytes contribute to murine spinal nerve transection-induced neuropathic pain. Eur J Immunol. 2008; 38(2):448–458. [PubMed: 18196515]
18. Caraher EM, Parenteau M, Gruber H, Scott FW. Flow cytometric analysis of intracellular IFN-gamma, IL-4 and IL-10 in CD3(+)4(+) T-cells from rat spleen. J Immunol Methods. 2000; 244(1–2):29–40. [PubMed: 11033016]

19. Chang MP, Yamaguchi DT, Yeh M, Taylor AN, Norman DC. Mechanism of the impaired T-cell proliferation in adult rats exposed to alcohol in utero. Int J Immunopharmacol. 1994; 16(4):345–357. [PubMed: 8045674]
20. Choi IY, Allan AM, Cunningham LA. Moderate fetal alcohol exposure impairs the neurogenic response to an enriched environment in adult mice. Alcohol Clin Exp Res. 2005; 29(11):2053–2062. [PubMed: 16340464]
21. Colleoni M, Sacerdote P. Murine models of human neuropathic pain. Biochim Biophys Acta. 2010; 1802(10):924–933. [PubMed: 19879943]
22. Costigan M, Moss A, Latremoliere A, Johnston C, Verma-Gandhu M, Herbert TA, Barrett L, Brenner GJ, Vardeh D, Woolf CJ, Fitzgerald M. T-cell infiltration and signaling in the adult dorsal spinal cord is a major contributor to neuropathic pain-like hypersensitivity. J Neurosci. 2009; 29(46):14415–14422. [PubMed: 19923276]
23. Couper KN, Blount DG, Riley EM. IL-10: the master regulator of immunity to infection. J Immunol. 2008; 180(9):5771–5777. [PubMed: 18424693]
24. Cunningham CL, Martinez-Cerdeno V, Noctor SC. Microglia regulate the number of neural precursor cells in the developing cerebral cortex. J Neurosci. 2013; 33(10):4216–4233. [PubMed: 23467340]
25. de la Rosa M, Rutz S, Dorninger H, Scheffold A. Interleukin-2 is essential for CD4+CD25+ regulatory T cell function. Eur J Immunol. 2004; 34(9):2480–2488. [PubMed: 15307180]
26. Dengler EC, Alberti LA, Bowman BN, Kerwin AA, Wilkerson JL, Moezzi DR, Limanovich E, Wallace JA, Milligan ED. Improvement of spinal non-viral IL-10 gene delivery by D-mannose as a transgene adjuvant to control chronic neuropathic pain. J Neuroinflammation. 2014; 11:92. [PubMed: 24884664]
27. DeVito WJ, Stone S. Prenatal exposure to ethanol alters the neuroimmune response to a central nervous system wound in the adult rat. Alcohol. 2001; 25(1):39–47. [PubMed: 11668016]
28. Drew PD, Johnson JW, Douglas JC, Phelan KD, Kane CJ. Pioglitazone blocks ethanol induction of microglial activation and immune responses in the hippocampus, cerebellum, and cerebral cortex in a mouse model of fetal alcohol spectrum disorders. Alcohol Clin Exp Res. 2015; 39(3):445–454. [PubMed: 25703036]
29. Echeverry S, Shi XQ, Rivest S, Zhang J. Peripheral nerve injury alters blood-spinal cord barrier functional and molecular integrity through a selective inflammatory pathway. J Neurosci. 2011; 31(30):10819–10828. [PubMed: 21795534]
30. Evans R, Patzak I, Svensson L, De Filippo K, Jones K, McDowall A, Hogg N. Integrins in immunity. J Cell Sci. 2009; 122(Pt 2):215–225. [PubMed: 19118214]
31. Fernandez-Lizarbe S, Pascual M, Guerri C. Critical role of TLR4 response in the activation of microglia induced by ethanol. J Immunol. 2009; 183(7):4733–4744. [PubMed: 19752239]
32. Foey AD, Brennan FM. Conventional protein kinase C and atypical protein kinase Czeta differentially regulate macrophage production of tumour necrosis factor-alpha and interleukin-10. Immunology. 2004; 112(1):44–53. [PubMed: 15096183]
33. Ford AL, Goodsall AL, Hickey WF, Sedgwick JD. Normal adult ramified microglia separated from other central nervous system macrophages by flow cytometric sorting. Phenotypic differences defined and direct ex vivo antigen presentation to myelin basic protein-reactive CD4+ T cells compared. J Immunol. 1995; 154(9):4309–4321. [PubMed: 7722289]
34. Franklin L, Deitz J, Jirikowic T, Astley S. Children with fetal alcohol spectrum disorders: problem behaviors and sensory processing. Am J Occup Ther. 2008; 62(3):265–273. [PubMed: 18557002]
35. Friedman TW, Robinson SR, Yelland GW. Impaired perceptual judgment at low blood alcohol concentrations. Alcohol. 2011; 45(7):711–718. [PubMed: 21145695]
36. Fuhl A, Muller-Dahlhaus F, Lucke C, Toennes SW, Ziemann U. Low Doses of Ethanol Enhance LTD-like Plasticity in Human Motor Cortex. Neuropsychopharmacology. 2015; 40(13):2969–2980. [PubMed: 26038159]
37. Gandler W, Shapiro H. Logarithmic amplifiers. Cytometry. 1990; 11(3):447–450. [PubMed: 2340779]
38. Gao YJ, Ji RR. Chemokines, neuronal-glial interactions, and central processing of neuropathic pain. Pharmacol Ther. 2010; 126(1):56–68. [PubMed: 20117131]

39. Gattlen C, Clarke CB, Piller N, Kirschmann G, Pertin M, Decosterd I, Gosselin RD, Suter MR. Spinal Cord T-Cell Infiltration in the Rat Spared Nerve Injury Model: A Time Course Study. Int J Mol Sci. 2016; 17(3):352. [PubMed: 27005622]
40. Gottesfeld Z, Morgan B, Perez-Polo JR. Prenatal alcohol exposure alters the development of sympathetic synaptic components and of nerve growth factor receptor expression selectivity in lymphoid organs. J Neurosci Res. 1990; 26(3):308–316. [PubMed: 2168949]
41. Gottesfeld Z, Ullrich SE. Prenatal alcohol exposure selectively suppresses cell-mediated but not humoral immune responsiveness. Int J Immunopharmacol. 1995; 17(3):247–254. [PubMed: 7558520]
42. Grace PM, Rolan PE, Hutchinson MR. Peripheral immune contributions to the maintenance of central glial activation underlying neuropathic pain. Brain Behav Immun. 2011; 25(7):1322–1332. [PubMed: 21496480]
43. Hamilton DA, Akers KG, Rice JP, Johnson TE, Candelaria-Cook FT, Maes LI, Rosenberg M, Valenzuela CF, Savage DD. Prenatal exposure to moderate levels of ethanol alters social behavior in adult rats: relationship to structural plasticity and immediate early gene expression in frontal cortex. Behav Brain Res. 2010; 207(2):290–304. [PubMed: 19852984]
44. Hashimoto S, Takahashi Y, Tomita Y, Hayama T, Sawada S, Horie T, McCombs CC, Michalski JP. Mechanism of calcium ionophore and phorbol ester-induced T-cell activation. Accessory cell requirement for T-cell activation. Scand J Immunol. 1991; 33(4):393–403. [PubMed: 2017664]
45. Hellemans KG, Sliwowska JH, Verma P, Weinberg J. Prenatal alcohol exposure: fetal programming and later life vulnerability to stress, depression and anxiety disorders. Neurosci Biobehav Rev. 2010; 34(6):791–807. [PubMed: 19545588]
46. Hettinger J, Richards DM, Hansson J, Barra MM, Joschko AC, Krijgsveld J, Feuerer M. Origin of monocytes and macrophages in a committed progenitor. Nat Immunol. 2013; 14(8):821–830. [PubMed: 23812096]
47. Huang D, Yu B. The mirror-image pain: an unclered phenomenon and its possible mechanism. Neurosci Biobehav Rev. 2010; 34(4):528–532. [PubMed: 19883682]
48. Hutchinson MR, Shavit Y, Grace PM, Rice KC, Maier SF, Watkins LR. Exploring the neuroimmunopharmacology of opioids: an integrative review of mechanisms of central immune signaling and their implications for opioid analgesia. Pharmacol Rev. 2011; 63(3):772–810. [PubMed: 21752874]
49. Jaggi AS, Jain V, Singh N. Animal models of neuropathic pain. Fundam Clin Pharmacol. 2011; 25(1):1–28.
50. Jancalek R. Signaling mechanisms in mirror image pain pathogenesis. Ann Neurosci. 2011; 18(3): 123–127. [PubMed: 25205938]
51. Josefowicz SZ, Lu LF, Rudensky AY. Regulatory T cells: mechanisms of differentiation and function. Annu Rev Immunol. 2012; 30:531–564. [PubMed: 22224781]
52. Jovanovic DV, Di Battista JA, Martel-Pelletier J, Jolicoeur FC, He Y, Zhang M, Mineau F, Pelletier JP. IL-17 stimulates the production and expression of proinflammatory cytokines, IL-beta and TNF-alpha, by human macrophages. J Immunol. 1998; 160(7):3513–3521. [PubMed: 9531313]
53. Kane CJ, Phelan KD, Drew PD. Neuroimmune mechanisms in fetal alcohol spectrum disorder. Dev Neurobiol. 2012; 72(10):1302–1316. [PubMed: 22623427]
54. Kim CF, Moalem-Taylor G. Detailed characterization of neuro-immune responses following neuropathic injury in mice. Brain Res. 2011; 1405:95–108. [PubMed: 21741621]
55. Kleinschnitz C, Brinkhoff J, Zelenka M, Sommer C, Stoll G. The extent of cytokine induction in peripheral nerve lesions depends on the mode of injury and NMDA receptor signaling. J Neuroimmunol. 2004; 149(1–2):77–83. [PubMed: 15020067]
56. Kleinschnitz C, Hofstetter HH, Meuth SG, Braeuninger S, Sommer C, Stoll G. T cell infiltration after chronic constriction injury of mouse sciatic nerve is associated with interleukin-17 expression. Exp Neurol. 2006; 200(2):480–485. [PubMed: 16674943]
57. Kobor MS, Weinberg J. Focus on: epigenetics and fetal alcohol spectrum disorders. Alcohol Res Health. 2011; 34(1):29–37. [PubMed: 23580038]
58. Koltzenburg M, Wall PD, McMahon SB. Does the right side know what the left is doing? Trends Neurosci. 1999; 22(3):122–127. [PubMed: 10199637]

59. Komatsu S, Sakata-Haga H, Sawada K, Hisano S, Fukui Y. Prenatal exposure to ethanol induces leptomeningeal heterotopia in the cerebral cortex of the rat fetus. Acta Neuropathol. 2001; 101(1): 22–26. [PubMed: 11194937]
60. Liao W, Lin JX, Leonard WJ. Interleukin-2 at the crossroads of effector responses, tolerance, and immunotherapy. Immunity. 2013; 38(1):13–25. [PubMed: 23352221]
61. Lin TH, Liu HH, Tsai TH, Chen CC, Hsieh TF, Lee SS, Lee YJ, Chen WC, Tang CH. CCL2 increases alphavbeta3 integrin expression and subsequently promotes prostate cancer migration. Biochim Biophys Acta. 2013; 1830(10):4917–4927. [PubMed: 23845726]
62. Mansfield JR. Multispectral imaging: a review of its technical aspects and applications in anatomic pathology. Vet Pathol. 2014; 51(1):185–210. [PubMed: 24129898]
63. Maxwell JR, Denson JL, Joste NE, Robinson S, Jantzie LL. Combined in utero hypoxia-ischemia and lipopolysaccharide administration in rats induces chorioamnionitis and a fetal inflammatory response syndrome. Placenta. 2015; 36(12):1378–1384. [PubMed: 26601766]
64. Milligan ED, O'Connor KA, Nguyen KT, Armstrong CB, Twining C, Gaykema RP, Holguin A, Martin D, Maier SF, Watkins LR. Intrathecal HIV-1 envelope glycoprotein gp120 induces enhanced pain states mediated by spinal cord proinflammatory cytokines. J Neurosci. 2001; 21(8): 2808–2819. [PubMed: 11306633]
65. Milligan ED, Watkins LR. Pathological and protective roles of glia in chronic pain. Nat Rev Neurosci. 2009; 10(1):23–36. [PubMed: 19096368]
66. Milner R, Campbell IL. The extracellular matrix and cytokines regulate microglial integrin expression and activation. J Immunol. 2003; 170(7):3850–3858. [PubMed: 12646653]
67. Montesinos J, Alfonso-Loeches S, Guerri C. Impact of the Innate Immune Response in the Actions of Ethanol on the Central Nervous System. Alcohol Clin Exp Res. 2016
68. Mosser DM, Zhang X. Activation of murine macrophages. Curr Protoc Immunol. 2008; Chapter 14(Unit 14):12.
69. Narita M, Miyoshi K, Narita M, Suzuki T. Involvement of microglia in the ethanol-induced neuropathic pain-like state in the rat. Neurosci Lett. 2007; 414(1):21–25. [PubMed: 17284346]
70. Norman DC, Chang MP, Wong CM, Branch BJ, Castle S, Taylor AN. Changes with age in the proliferative response of splenic T cells from rats exposed to ethanol in utero. Alcohol Clin Exp Res. 1991; 15(3):428–432. [PubMed: 1877729]
71. Perkins NM, Tracey DJ. Hyperalgesia due to nerve injury: role of neutrophils. Neuroscience. 2000; 101(3):745–757. [PubMed: 11113323]
72. Perrin FE, Lacroix S, Aviles-Trigueros M, David S. Involvement of monocyte chemoattractant protein-1, macrophage inflammatory protein-1alpha and interleukin-1beta in Wallerian degeneration. Brain. 2005; 128(Pt 4):854–866. [PubMed: 15689362]
73. Portales-Casamar E, Lussier AA, Jones MJ, MacIsaac JL, Edgar RD, Mah SM, Barhdadi A, Provost S, Lemieux-Perreault LP, Cynader MS, Chudley AE, Dube MP, Reynolds JN, Pavlidis P, Kobor MS. DNA methylation signature of human fetal alcohol spectrum disorder. Epigenetics Chromatin. 2016; 9:25. [PubMed: 27358653]
74. Prasad, PN. Wiley InterScience (Service en ligne). Introduction to biophotonics. Hoboken, N.J: Wiley-Interscience; 2004.
75. Ransohoff RM, Kivisakk P, Kidd G. Three or more routes for leukocyte migration into the central nervous system. Nat Rev Immunol. 2003; 3(7):569–581. [PubMed: 12876559]
76. Redei E, Clark WR, McGivern RF. Alcohol exposure in utero results in diminished T-cell function and alterations in brain corticotropin-releasing factor and ACTH content. Alcohol Clin Exp Res. 1989; 13(3):439–443. [PubMed: 2546466]
77. Robinson S, Berglass JB, Denson JL, Berkner J, Anstine CV, Winer JL, Maxwell JR, Qiu J, Yang Y, Sillerud LO, Meehan WP 3rd, Mannix R, Jantzie LL. Microstructural and microglial changes after repetitive mild traumatic brain injury in mice. J Neurosci Res. 2016
78. Romero-Sandoval A, Chai N, Nutile-McMenemy N, Deleo JA. A comparison of spinal Iba1 and GFAP expression in rodent models of acute and chronic pain. Brain Res. 2008; 1219:116–126. [PubMed: 18538310]
79. Romero-Sandoval EA, Horvath RJ, DeLeo JA. Neuroimmune interactions and pain: focus on glial-modulating targets. Curr Opin Investig Drugs. 2008; 9(7):726–734.

80. Rothhammer V, Heink S, Petermann F, Srivastava R, Claussen MC, Hemmer B, Korn T. Th17 lymphocytes traffic to the central nervous system independently of alpha4 integrin expression during EAE. J Exp Med. 2011; 208(12):2465–2476. [PubMed: 22025301]
81. Ruohonen S, Jagodi M, Khademi M, Taskinen HS, Ojala P, Olsson T, Roytta M. Contralateral non-operated nerve to transected rat sciatic nerve shows increased expression of IL-1beta, TGF-beta1, TNF-alpha, and IL-10. J Neuroimmunol. 2002; 132(1–2):11–17. [PubMed: 12417428]
82. Sabat R, Grutz G, Warszawska K, Kirsch S, Witte E, Wolk K, Geginat J. Biology of interleukin-10. Cytokine Growth Factor Rev. 2010; 21(5):331–344. [PubMed: 21115385]
83. Savage DD, Rosenberg MJ, Wolff CR, Akers KG, El-Emawy A, Staples MC, Varaschin RK, Wright CA, Seidel JL, Caldwell KK, Hamilton DA. Effects of a novel cognition-enhancing agent on fetal ethanol-induced learning deficits. Alcohol Clin Exp Res. 2010; 34(10):1793–1802. [PubMed: 20626729]
84. Schmitt KU, Lanz C, Muser MH, Walz F, Schwarz U. Saccadic eye movements after low-dose oral alcohol exposure. J Forensic Leg Med. 2013; 20(7):870–874. [PubMed: 24112339]
85. Schneider ML, Moore CF, Adkins MM. The effects of prenatal alcohol exposure on behavior: rodent and primate studies. Neuropsychol Rev. 2011; 21(2):186–203. [PubMed: 21499982]
86. Schneider ML, Moore CF, Barnhart TE, Larson JA, DeJesus OT, Mukherjee J, Nickles RJ, Converse AK, Roberts AD, Kraemer GW. Moderate-level prenatal alcohol exposure alters striatal dopamine system function in rhesus monkeys. Alcohol Clin Exp Res. 2005; 29(9):1685–1697. [PubMed: 16205369]
87. Schneider ML, Moore CF, Gajewski LL, Larson JA, Roberts AD, Converse AK, DeJesus OT. Sensory processing disorder in a primate model: evidence from a longitudinal study of prenatal alcohol and prenatal stress effects. Child Dev. 2008; 79(1):100–113. [PubMed: 18269511]
88. Scholz J, Woolf CJ. The neuropathic pain triad: neurons, immune cells and glia. Nat Neurosci. 2007; 10(11):1361–1368. [PubMed: 17965656]
89. Schuerwegh AJ, Stevens WJ, Bridts CH, De Clerck LS. Evaluation of monensin and brefeldin A for flow cytometric determination of interleukin-1 beta, interleukin-6, and tumor necrosis factor-alpha in monocytes. Cytometry. 2001; 46(3):172–176. [PubMed: 11449408]
90. Schutte RJ, Parisi-Amon A, Reichert WM. Cytokine profiling using monocytes/macrophages cultured on common biomaterials with a range of surface chemistries. J Biomed Mater Res A. 2009; 88(1):128–139. [PubMed: 18260130]
91. Sedgwick JD, Schwender S, Imrich H, Dorries R, Butcher GW, ter Meulen V. Isolation and direct characterization of resident microglial cells from the normal and inflamed central nervous system. Proc Natl Acad Sci U S A. 1991; 88(16):7438–7442. [PubMed: 1651506]
92. Soderquist RG, Sloane EM, Loram LC, Harrison JA, Dengler EC, Johnson SM, Amer LD, Young CS, Lewis MT, Poole S, Frank MG, Watkins LR, Milligan ED, Mahoney MJ. Release of plasmid DNA-encoding IL-10 from PLGA microparticles facilitates long-term reversal of neuropathic pain following a single intrathecal administration. Pharm Res. 2010; 27(5):841–854. [PubMed: 20224990]
93. Sorge RE, Mapplebeck JC, Rosen S, Beggs S, Taves S, Alexander JK, Martin LJ, Austin JS, Sotocinal SG, Chen D, Yang M, Shi XQ, Huang H, Pillon NJ, Bilan PJ, Tu Y, Klip A, Ji RR, Zhang J, Salter MW, Mogil JS. Different immune cells mediate mechanical pain hypersensitivity in male and female mice. Nat Neurosci. 2015; 18(8):1081–1083. [PubMed: 26120961]
94. Spataro LE, Sloane EM, Milligan ED, Wieseler-Frank J, Schoeniger D, Jekich BM, Barrientos RM, Maier SF, Watkins LR. Spinal gap junctions: potential involvement in pain facilitation. J Pain. 2004; 5(7):392–405. [PubMed: 15501197]
95. Squarzoni P, Oller G, Hoeffel G, Pont-Lezica L, Rostaing P, Low D, Bessis A, Ginhoux F, Garel S. Microglia modulate wiring of the embryonic forebrain. Cell Rep. 2014; 8(5):1271–1279. [PubMed: 25159150]
96. Starnes T, Robertson MJ, Sledge G, Kelich S, Nakshatri H, Broxmeyer HE, Hromas R. Cutting edge: IL-17F, a novel cytokine selectively expressed in activated T cells and monocytes, regulates angiogenesis and endothelial cell cytokine production. J Immunol. 2001; 167(8):4137–4140. [PubMed: 11591732]

97. Sweitzer SM, White KA, Dutta C, DeLeo JA. The differential role of spinal MHC class II and cellular adhesion molecules in peripheral inflammatory versus neuropathic pain in rodents. J Neuroimmunol. 2002; 125(1–2):82–93. [PubMed: 11960644]

98. Taskinen HS, Roytta M. Increased expression of chemokines (MCP-1, MIP-1alpha, RANTES) after peripheral nerve transection. J Peripher Nerv Syst. 2000; 5(2):75–81. [PubMed: 10905466]

99. Tawfik VL, Nutile-McMenemy N, Lacroix-Fralish ML, Deleo JA. Efficacy of propentofylline, a glial modulating agent, on existing mechanical allodynia following peripheral nerve injury. Brain Behav Immun. 2007; 21(2):238–246. [PubMed: 16949251]

100. Terasaki LS, Schwarz JM. Effects of Moderate Prenatal Alcohol Exposure during Early Gestation in Rats on Inflammation across the Maternal-Fetal-Immune Interface and Later-Life Immune Function in the Offspring. J Neuroimmune Pharmacol. 2016

101. Tewari S, Diano M, Bera R, Nguyen Q, Parekh H. Alterations in brain polyribosomal RNA translation and lymphocyte proliferation in prenatal ethanol-exposed rats. Alcohol Clin Exp Res. 1992; 16(3):436–442. [PubMed: 1626642]

102. Tiwari V, Chopra K. Resveratrol prevents alcohol-induced cognitive deficits and brain damage by blocking inflammatory signaling and cell death cascade in neonatal rat brain. J Neurochem. 2011; 117(4):678–690. [PubMed: 21375533]

103. Topper LA, Baculis BC, Valenzuela CF. Exposure of neonatal rats to alcohol has differential effects on neuroinflammation and neuronal survival in the cerebellum and hippocampus. J Neuroinflammation. 2015; 12:160. [PubMed: 26337952]

104. Valenzuela CF, Morton RA, Diaz MR, Topper L. Does moderate drinking harm the fetal brain? Insights from animal models. Trends Neurosci. 2012; 35(5):284–292. [PubMed: 22402065]

105. Verhagen J, Wraith DC. Blockade of LFA-1 augments in vitro differentiation of antigen-induced Foxp3(+) Treg cells. J Immunol Methods. 2014; 414:58–64. [PubMed: 25108241]

106. Wagner C, Hansch GM, Stegmaier S, Denefleh B, Hug F, Schoels M. The complement receptor 3, CR3 (CD11b/CD18), on T lymphocytes: activation-dependent up-regulation and regulatory function. Eur J Immunol. 2001; 31(4):1173–1180. [PubMed: 11298342]

107. Wallace JA, Romero AA, Gabaldon AM, Roe VA, Saavedra SL, Lobner J. Tyrosine hydroxylase-containing neurons in the spinal cord of the chicken. I. Development and analysis of catecholamine synthesis capabilities. Cell Mol Neurobiol. 1996; 16(6):625–648. [PubMed: 9013027]

108. Wang Y, Kai H, Chang F, Shibata K, Tahara-Hanaoka S, Honda S, Shibuya A, Shibuya K. A critical role of LFA-1 in the development of Th17 cells and induction of experimental autoimmune encephalomyelytis. Biochem Biophys Res Commun. 2007; 353(4):857–862. [PubMed: 17207459]

109. Weinberg J, Sliwowska JH, Lan N, Hellemans KG. Prenatal alcohol exposure: foetal programming, the hypothalamic-pituitary-adrenal axis and sex differences in outcome. J Neuroendocrinol. 2008; 20(4):470–488. [PubMed: 18266938]

110. Wilkerson JL, Gentry KR, Dengler EC, Wallace JA, Kerwin AA, Armijo LM, Kuhn MN, Thakur GA, Makriyannis A, Milligan ED. Intrathecal cannabilactone CB(2)R agonist, AM1710, controls pathological pain and restores basal cytokine levels. Pain. 2012; 153(5):1091–1106. [PubMed: 22425445]

111. Wilkerson JL, Gentry KR, Dengler EC, Wallace JA, Kerwin AA, Kuhn MN, Zvonok AM, Thakur GA, Makriyannis A, Milligan ED. Immunofluorescent spectral analysis reveals the intrathecal cannabinoid agonist, AM1241, produces spinal anti-inflammatory cytokine responses in neuropathic rats exhibiting relief from allodynia. Brain Behav. 2012; 2(2):155–177. [PubMed: 22574283]

112. Zhang Y, Wang H. Integrin signalling and function in immune cells. Immunology. 2012; 135(4): 268–275. [PubMed: 22211918]

113. Zhang ZJ, Cao DL, Zhang X, Ji RR, Gao YJ. Chemokine contribution to neuropathic pain: respective induction of CXCL1 and CXCR2 in spinal cord astrocytes and neurons. Pain. 2013; 154(10):2185–2197. [PubMed: 23831863]

Highlights

- Moderate prenatal alcohol exposure (PAE) potentiates adult-onset sciatic nerve damage- induced chronic neuropathic pain.
- PAE induces exaggerated glial activation in the anatomically relevant spinal cord region (lumbar spinal cord) following peripheral nerve injury.
- PAE increases major histocompatibility complex II (MHCII) and β-integrin adhesion molecules-expressing spinal glia and leukocytes, indicative of PAE related spinal immune cell activation.
- PAE potentiates pro-inflammatory cytokine levels in the sciatic nerve ipsilateral to chronic constriction injury.
- Blunted IL-10 levels were detected in the ipsilateral sciatic nerve and corresponding dorsal root ganglia in neuropathic PAE offspring.

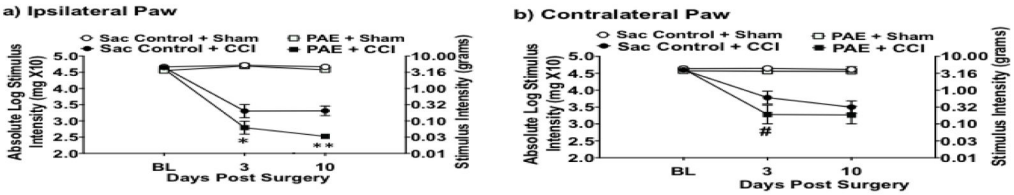

Figure 1. Prenatal alcohol exposure (PAE) potentiates allodynia in adult rats following Chronic Constriction Injury (CCI)

Absolute threshold behavioral responses for (a) ipsilateral and (b) contralateral hindpaws are shown. At baseline (BL), responses to low threshold mechanical stimuli were similar in all groups (ipsilateral, $F_{1,36}$= 1.877, P =0.179; contralateral, $F_{1,36}$= 1.228, P = 0.275), regardless of PAE or saccharin (Sac) treatment. Statistics show a main effect of alcohol exposure from data collected from the ipsilateral hindpaw [$F_{1,36}$ = 12.009, P = 0.001] but not in the contralateral hindpaw [$F_{1,36}$ = 4.169, P = 0.049]. There was a main effect of CCI surgery [ipsilateral, $F_{1,36}$ = 311.943, P < 0.001; contralateral, $F_{1,36}$ = 54.554, P < 0.001]. In addition, an interaction between alcohol exposure and CCI surgery only in the ipsilateral hindpaw [ipsilateral, $F_{1,36}$ = 5.246, P = 0.028; contralateral, $F_{1,36}$ = 1.383, P = 0.247] is observed. Comparison of treatment groups post-surgery demonstrate a larger increase in sensitivity following CCI in PAE animals compared to their Sac-CCI counterparts where a main effect of alcohol exposure in the ipsilateral hindpaw [ipsilateral, $F_{1,36}$ = 12.938, P = 0.001; contralateral, $F_{1,36}$ = 4.003, P = 0.053] is observed. In addition, a main effect of CCI surgery [ipsilateral, $F_{1,36}$ = 347.595, P < 0.001; contralateral, $F_{1,36}$ = 58.406, P < 0.001] and an interaction of alcohol exposure and CCI surgery in the ipsilateral paw [ipsilateral, $F_{1,36}$ = 8.312, P = 0.007; contralateral, $F_{1,36}$ = 1.928, P = 0.174] was revealed. N=10 rats in each group.

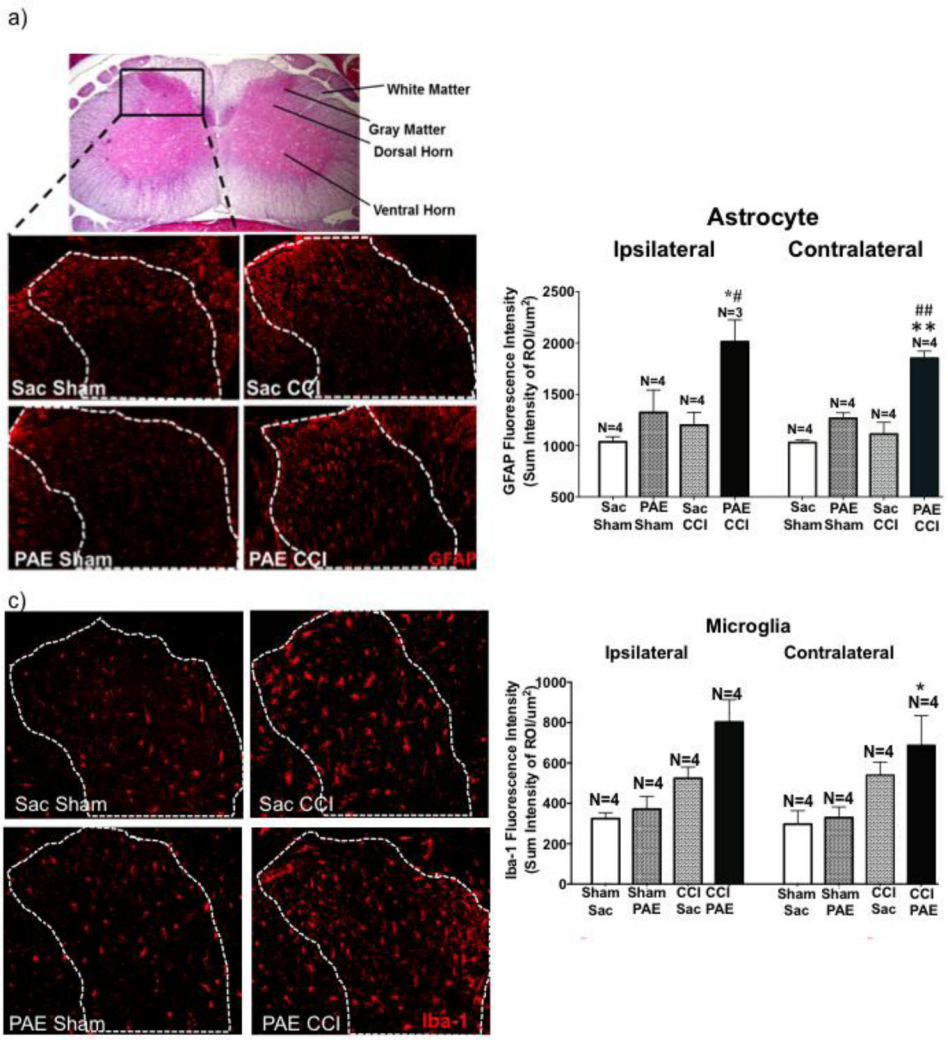

Figure 2. PAE results in heightened glial activation following CCI

Immunohistochemical (IHC) quantification was used to assess activation of astrocytes (GFAP) and microglia/macrophages (Iba1) in squad 2 animals. Images analyzed contained only true signal (i.e. fluorescence outside the spectrum of interest was omitted). The sum intensity within the region of interest (i.e. lumbar spinal cord dorsal horn) was used to determine overall activation. (a) Top panel: representative cross-section of an H&E stained L4 spinal cord with the dorsal horn subjected to analysis outlined in the black box. Lower panels: GFAP stained lumbar spinal cord sections (ipsilateral) from each experimental condition with images taken using a 20X objective. (b) Image analysis of acquired IR images that include the representative images in (a). PAE-CCI treated spinal cords display exaggerated astrocyte activation. PAE treatment elevates GFAP (ipsilateral: $F_{1,11} = 6.885$, $P = 0.0237$; contralateral: $F_{1,12} = 20.55$, $P = 0.0007$) and CCI elevates GFAP (ipsilateral: $F_{1,11} = 11.49$, $P = 0.0060$; contralateral: $F_{1,12} = 43.88$, $P < 0.0001$). Compared to PAE sham treatment, GFAP IR is elevated in PAE with CCI (95% CI: ipsilateral [−1340, −290], #P=0.0058 and contralateral [−967.3, −513], ##P<0.0001). Additionally, compared to Sac CCI treatment, GFAP IR is significantly elevated in PAE with CCI treatment (95% CI:

ipsilateral [−1215, −165.5], *P=0.0146 and contralateral [−813.2, −359], **P=0.0001). N = 3–4 rats per group. (c) Representative Iba-1 (microglia) stained lumbar spinal cord sections (ipsilateral) from each experimental condition, images taken with a 20X objective. (d) Image analysis of acquired IR images that include the representative images in (c). While Iba-1 IR is significantly increased in animals with chronic allodynia (ipsilateral: $F_{1,12}$ = 19.52; P = 0.0008; contralateral, $F_{1,12}$ = 11.01, P = 0.0061), PAE also significantly increased Iba-1 IR (ipsilateral, $F_{1,12}$ =5.197, P = 0.0417). PAE-CCI animals displayed significantly heightened microglial activation compared to Sac-Shams (95% CI: ipsilateral [−698.2, −258.2], *P=0.0005 and contralateral [−670.1, −111.4], *P=0.01) and to Sac-CCI (95% CI: ipsilateral [−498.7, −58.75], $^{\#}$P = 0.017). N = 4 rats per group.

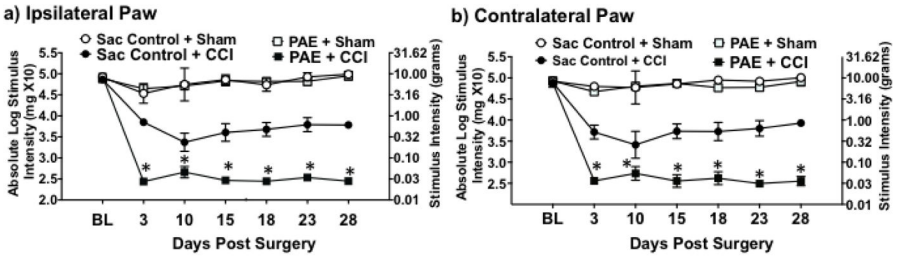

Figure 3. PAE potentiates chronic allodynia

At baseline (BL), (a) ipsilateral and (b) contralateral threshold responses are similar between all groups (ipsilateral, $F_{1,16} = 1.209$, $P = 0.288$; contralateral, $F_{1,16} = .036$, $P = 0.852$). Following CCI surgery, both PAE and Sac control animals displayed significantly increased hindpaw sensitivity on Days 3, 10, 15, 18, 23, and 28 post-surgery where there was a main effect of alcohol exposure [ipsilateral, $F_{1,16} = 84.616$, $P < 0.001$; contralateral, $F_{1,16} = 138.980$, $P < 0.001$], CCI surgery [ipsilateral, $F_{1,16} = 787.072$, $P < 0.001$; contralateral, $F_{1,16} = 1180.917$, $P < 0.001$], and an interaction between alcohol exposure and CCI surgery [ipsilateral, $F_{1,16} = 82.506$, $P < 0.001$; contralateral, $F_{1,16} = 103.264$, $P < 0.001$]. Compared to Sac animals, PAE animals displayed the greatest degree of hindpaw sensitivity following CCI surgery where a main effect of alcohol exposure [ipsilateral, $F_{1,16} = 93.167$, $P < 0.001$; contralateral, $F_{1,16} = 149.318$, $P < 0.001$], CCI surgery [ipsilateral, $F_{1,16} = 857.901$, $P < 0.001$; contralateral, $F_{1,16} = 1258.469$, $P < 0.001$] is observed, and an interaction between alcohol exposure and CCI surgery [ipsilateral, $F_{1,16} = 92.780$, $P < 0.001$; contralateral, $F_{1,16} = 110.212$, $P < 0.001$].

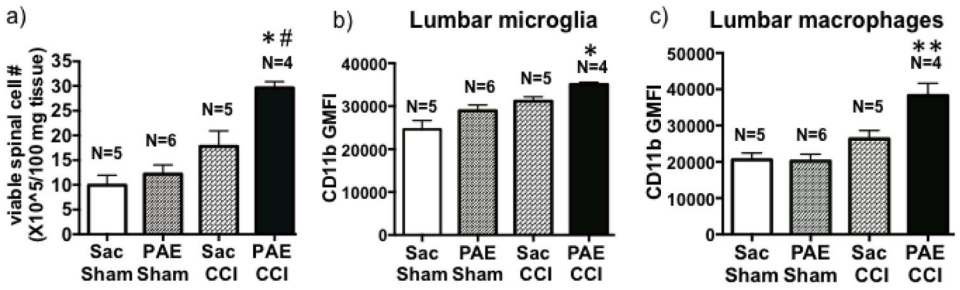

Figure 4. PAE alters cellular activation of microglia/macrophages in animal with chronic allodynia

Lumbar spinal cord tissues were collected on Day 28 post-surgery and a spinal cord single cell suspension was generated. (a) The total number of viable spinal glia/leukocytes was increased in CCI animals compared to Sham-treated animals, with the most robust increase observed in PAE-CCI compared to Sac-Sham (95% CI: [−29.39, −9.983], # p=0.0001) and Sac-CCI (95% CI: [−21.55, −2.143], *p=0.0143). (b) CD11b geometric mean fluorescence intensity (GMFI) for lumbar microglia ($CD11b^{high}CD45^{low\text{-}med}$) is increased following CCI (a main effect of CCI; $F_{1, 16} = 19.2$, P = 0.0005) and PAE (a main effect of PAE; $F_{1, 16} = 8.0$, P = 0.01) with the greatest increase observed in PAE + CCI treated rats (95% CI: [−15009, −5895], * p=0.0002 compared to Sac-Sham), indicating augmented microglial action. (c) The GMFI in macrophages ($CD11b^{high}CD45^{hi}$) is significantly upregulated following CCI (a main effect of CCI; $F_{1, 16} = 25.5$, P = 0.0001) and PAE (a main effect of PAE; $F_{1, 16} = 6.03$, P = 0.02), with significantly increased CD11b intensity observed in PAE + CCI compared to those from Sac-CCI animals (95% CI: [−19325, −4517], **P < 0.003). Data are presented as mean ± SEM, numbers of animals used are indicated on each bar.

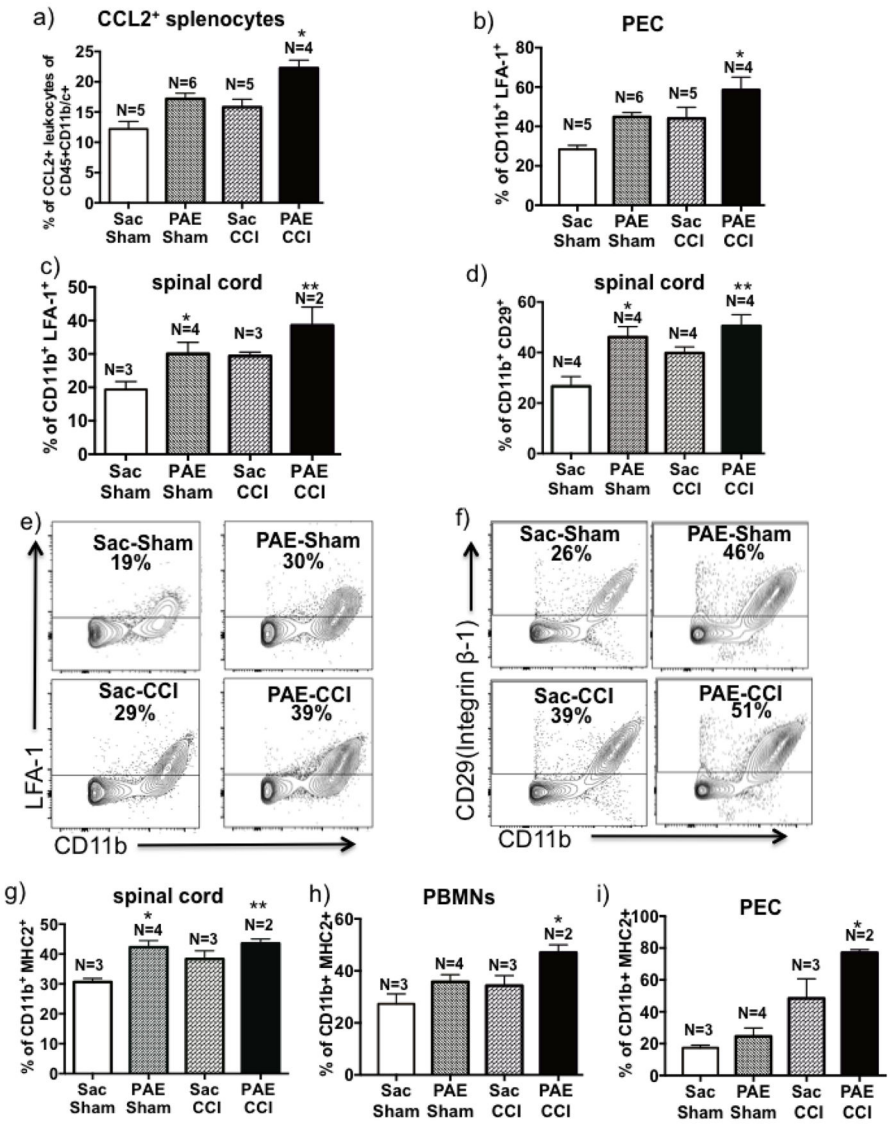

Figure 5. Expression of CCL2, integrins and MHC2 are altered in CD11b$^+$ cells in PAE animals with chronic allodynia

(a) Splenic cells were stimulated with PMA/Ionomycin *in vitro* and intracellular CCL2 were detected by flow cytometry. Bar graph represents percent of CCL2$^+$CD45$^+$CD11b$^+$ leukocytes indicating both PAE ($F_{1,16}$ = 22.5, P = 0.0002) and neuropathy ($F_{1,16}$ = 13.5, P = 0.002) significantly induced CCL2 expression. The greatest increase in CCL2$^+$ leukocytes were observed in PAE-CCI group, compared to Sac-CCI animals (95% CI: [−10.2, −2.67], *P = 0.002). (b) Data of LFA-1$^+$CD11b$^+$ cellular proportions are represented as a bar graph, which reveals significant increase in LFA-1 positivity on CD11b$^+$ PECs under chronic CCI-induced neuropathy ($F_{1,16}$ = 11.8, P = 0.003) and in PAE-treated rats ($F_{1,16}$ = 13.2, P=0.002). The LFA-1$^+$ CD11b$^+$ cells were significantly increased in PAE-CCI group, compared to Sac-CCI animals (95% CI: [−27.8, −1.12], *P = 0.03). (c) Live CD11b$^+$ spinal leukocytes were analyzed for expression of LFA-1. Data of LFA-1$^+$Cd11b$^+$ scatterplot proportions are represented as a bar graph revealing increase in LFA-1 positivity on lumbar

immune cells under chronic CCI-induced neuropathy ($F_{1,8}$ = 8.891, P = 0.017) and in PAE-treated rats ($F_{1,8}$ = 7.736, P=0.02). The LFA-1^+ $CD11b^+$ cells were significantly increased in PAE-treated group, *P=0.03 and **P=0.005 compared to Sac-Sham. (d) Data of CD29 scatterplot proportions are represented as a bar graph, revealing CD29 is significantly upregulated in animals under CCI-induced neuropathic conditions ($F_{1, 12}$ = 5.24, P = 0.045) and also in those with PAE treatment ($F_{1, 12}$ = 15.69, P = 0.0019), *P=0.003 and **P=0.0008 compared to Sac-Sham group. (e) Representative LFA-1 vs. CD11b scatterplots (from two independent experiments) for each condition are shown. The mean proportion of $CD11b^+LFA\text{-}1^+$ cells is indicated as a percentage. (f) Representative CD29 vs. CD11b scatterplots (from two independent experiments) are shown with the mean proportion of $CD11b^+CD29^+$ cells indicated as a percentage. (g) Bar graph of proportions of $CD11b^+MHC2^+$ cells in lumber spinal cord. PAE significantly induced MHCII expression ($F_{1,8}$ = 13.59, P = 0.0062), *P=0.004 and **P=0.006 compared to Sac-Sham group. h) Bar graph of $CD11b^+MHC2^+$ on peripheral blood mononuclear cells (PBMNs). Both PAE and neuropathy significantly induced MHCII expression on PBMNs ($F_{1,8}$ = 8.7, P = 0.02 for PAE and $F_{1,8}$ = 6.5, P = 0.03 for neuropathy). *P=0.03 compared to Sac-Sham group. i) Bar graph of $CD11b^+MHC2^+$ on peritoneal exudate cells (PEC). MHC2 expression is increased on PECs following PAE ($F_{1,8}$ = 5.6, P = 0.04) and following neuropathy ($F_{1,8}$ = 30.5, P = 0.006). A significant increase of MHC2 expression was observed in PAE+CCI rats, compared to Sac-CCI group, (95% CI: [−55.4, −1.9], *P=0.039). All bar graphs are presented as mean ± SEM, numbers of animals used are indicated on each bar.

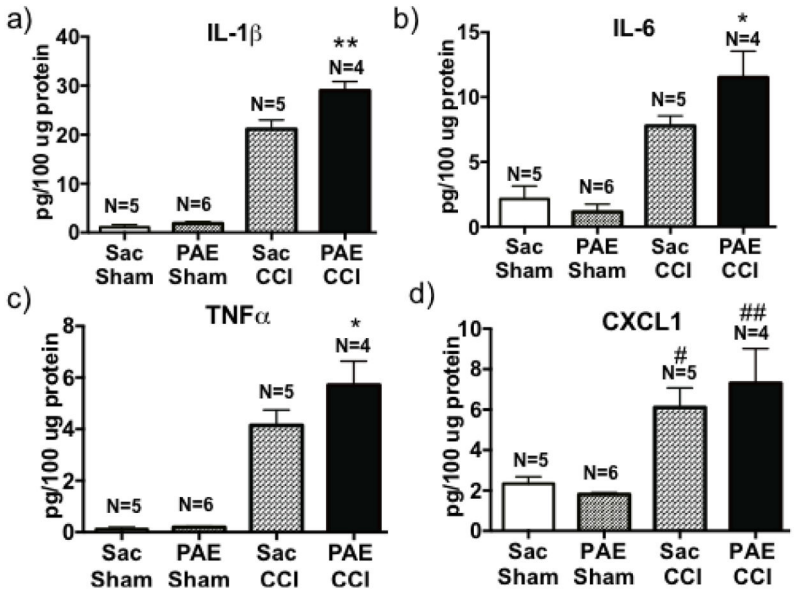

Figure 6. PAE animals express higher levels of proinflammatory mediators in the sciatic nerve (SCN) following neuropathy

Ipsilateral SCNs were collected on Day 28 after surgery and examined by multiplex protein analysis for levels of proinflammatory cytokines and the chemokine, CXCL1. Protein content is represented as picograms of target protein per 100μg of total protein. Data for (a) interleukin-1β (IL-1β), (b) IL-6, (c) tumor necrosis factor α (TNFα) and (d) C-X-C motif chemokine ligand 1 (CXCL1) protein content are represented. Proinflammatory cytokines were significantly increased in CCI-induced neuropathic animals, specifically for IL-1β ($F_{1, 16} = 361.9$, $P < 0.0001$), IL-6 ($F_{1, 16} = 54.7$, $P < 0.0001$), TNFα ($F_{1, 16} = 100.7$, $P < 0.0001$) and CXCL1 ($F_{1, 16} = 29.69$, $P < 0.0001$). CXCL1 levels increased significantly in Sac-CCI and PAE-CCI group, #P=0.006 compared to Sac-Sham group and ##P=0.0003, compared to PAE-Sham. Moreover, PAE-CCI animals expressed the greatest increase in protein IL-1β, IL-6 and TNFα levels compared to Sac-CCI animals (95% CI: IL-1β [−11.77, −3.96]; IL-6 [−7.14, −0.32] and TNFα [−3.06, −0.072], *P = 0.04, **P = 0.006). Data are presented as mean ± SEM [103].

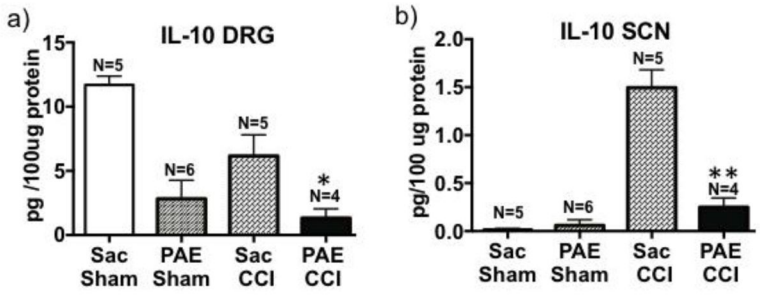

Figure 7. Interleukin-10 protein expression is dysregulated the sciatic nerve and DRG in neuropathic PAE animals

Ipsilateral SCN and ipsilateral lumbar (L4-L6) dorsal root ganglia (DRGs) were collected on Day 28 post-surgery and analyzed for IL-10 using multiplex protein analysis. IL-10 protein content is represented as picograms of IL-10 per 100μg of total protein. (a) Following examination of ipsilateral DRG IL-10 levels, a main effect of PAE ($F_{1,15}$ = 5.13, P = 0.0002) and CCI ($F_{1, 15}$ = 6.61, P = 0.02) was observed with a blunting IL-10 expression. The lowest levels of DRG IL-10 protein were observed in PAE-CCI treated rats compared to Sac-treated CCI rats (95%CI: [2.679, 9.820], *P = 0.02). (b) IL-10 protein content in ipsilateral SCNs demonstrate a significant compensatory increase in IL-10 levels in nerves from Sac-treated rats with CCI-induced neuropathy ($F_{1,16}$ = 61.65, P < 0.0001). However SCNs from PAE rats expressed far less protein IL-10 ($F_{1,16}$ = 32.23, P < 0.0001), with the most diminished IL-10 levels observed in PAE- CCI rats compared to Sac-CCI [95%CI: 0.916, 1.59], **P < 0.0001). Data are presented as ± SEM.